ADVANCED GEOMATICS

E-ISSN: 2791-8637

Volume: 3
Issue: 2
September, 2023

Advanced Geomatics

About Journal

The Advanced Geomatics Journal (AGE) covers all aspects and information on scientific and technical advances in the geomatics sciences. AGE publishes original and innovative contributions in geomatics applications ranging from the integration of instruments, methodologies, and technologies and their respective uses in the environmental sciences, engineering, and other natural sciences.
AGE is a double-blind peer-review journal. At least two reviewers, professionals in their field of specialization, evaluate the original article after the study was checked in iThenticate ® (Professional Plagiarism Prevention) software.

Aim & Scope

The scope of Advanced Geomatics;

- ✓ B All multidisciplinary studies with UAV
- ✓ Application of Geomatics
- ✓ Augmented Reality and Virtual Reality Applications with UAV
- ✓ Cartography
- ✓ Construction Surveys
- ✓ Crowdsourcing/volunteered geographic information
- ✓ Deformation and Landslide Measurements with UAV
- ✓ Deformation Measurements
- ✓ Digital Mapping
- ✓ Documentation Studies with UAV
- ✓ Geodesy
- ✓ Geodetic and Control Surveys
- ✓ Geographical Information Systems
- ✓ Geographical Information Systems Applications with UAV
- ✓ GNSS and GPS
- ✓ Hydrography
- ✓ Image Processing and Analysis
- ✓ Indoor navigation
- ✓ Industrial Measurements with UAV
- ✓ Land Information Systems (LIS)
- ✓ Mining Measurements with UAV
- ✓ Photogrammetry
- ✓ Positioning and navigation
- ✓ Precision Agriculture Practices with UAV
- ✓ Remote Sensing
- ✓ Sensors
- ✓ Spatial Data Analysis
- ✓ Spatial Information Science
- ✓ UAV LiDAR and Applications
- ✓ UAV Photogrammetry and Remote Sensing with UAV
- ✓ Urban Planning and Transportation Planning Studies with UAV

Publication frequency Biannual
WEB http://publish.mersin.edu.tr/index.php/geomatics/index
Contact myakar@mersin.edu.tr / aliulvi@mersin.edu.tr / ayasinyigit@mersin.edu.tr

Advanced Geomatics

Advanced Geomatics
Volume *3*
Issue *2* *September, 2023*

Contents

Research Articles;

Advanced Geomatics

http://publish.mersin.edu.tr/index.php/geomatics/index

e-ISSN: 2791-8637

GLOF Hazard Assessment using Geospatial Techniques in Hunza Nagar, Gilgit Baltistan, Pakistan

Ahsan Iqbal[1], Shakeel Mahmood*[1]

[1]Department of Geography, Government College University Lahore, 54000, Lahore, Pakistan; (ahsaniqbal715571@gmail.com; shakeelmahmoodkhan@gmail.com)

Keywords

GLOF hazard,
Risk assesment,
Glacial retreat,
Hunza Nagar,
Karakoram anomaly.

Research Article

Received : 18.03.2023
Revised : 08.09.2023
Accepted : 11.09.2023
Published : 30.09.2023

* **Corresponding Author**
shakeelmahmoodkhan@gmail.com

Abstract

Worldwide in different regions, increase in temperature has caused variations in many natural phenomena particularly expansion, contraction and creation of glacial lakes Hindu Kush Himalayas (HKH) region. In the recent past, several of these lakes have been burst out and generated Glacial Lake Outburst Floods (GLOFs) causing considerable human life loss damages to infrastructure and properties in downstream areas. This study is an effort to assess GLOF hazard in Nagar valley, Gilgit Baltistan using Geo-spatial Technique. Shuttle Radar Topographic Mission (SRTM) Digital Elevation Model (DEM) and Google Earth image has been utilized as input data. Buffer analysis is applied to demarcate the hazard zone and map the elements at risk. The results indicated that Passu Lake has potential to cause GLOF. The volume of the lake has been increased from 788383.79 m^3 (2016) to 892910.494 m^3 (2018). The exposed areas include portions of Karakoram Highway and some villages downstream to Passu Lake along Hunza River. The outcomes of this study will be helpful in reducing the adverse impacts of GLOFs events in Passu sub-watershed. The results can also assist decision makers to develop a mechanism for reliable and cost effective monitoring of glacier lakes and GLOFs hazard and risk assessment using advance geospatial hydrologic/hydraulic modeling techniques.

1. Introduction

Globally, there is a general trend of mountain glacier recession and thinning in response to global warming and climate change. Receding glaciers give rise to glacial lakes when melt water gets accumulated behind semi-permanent structures like moraines and ice. Bursting of these lakes by sudden breach in moraine or ice can cause Glacial Lake Outburst Floods (GLOFs) in the downstream areas. Increase in temperature has caused variations in many natural phenomena particularly expansion, contraction and creation of glacial lakes Hindu Kush Himalayas (HKH) region. GLOFs are causing considerable human life loss, damages to infrastructure and properties in downstream areas (Mernild et al. 2015). The key contributing factors to GLOF hazard and its monitoring are remote sensing, lake volume and rate of formation, reaction of glacier to climatic parameters, activity of glacier, possibility of mass moments into lake, stability, width and height of moraine, and nature and situation down valley. Glacial lakes receive melt-water from parent glacier and related to availability of ice and temperature. The sudden outburst of glacial lakes causes GLOF in downstream area (Pinglot et al. 1994). Consequently, damages to both people and property occur. It is important to keep an eye on the condition of these lakes. Traditional surveys find it very challenging to monitor because of their remote locations and high altitudes (Mool 1995). Since most of the factors connected to glacial lakes can be analyzed using remote sensing data (Bolch et al. 2008). The volume and rate of lake formation, the glacier's response to the climate, its activity, the potential for mass moments into the lake, stability, the width and height of the moraine, and the

Cite this;

Iqbal, A. & Mahmood, S. (2023). GLOF Hazard Assessment using Geospatial Techniques in Hunza Nagar, Gilgit Baltistan, Pakistan. Advanced Geomatics, 3(2), 40-46.

location down valley are the main contributors to glacial lake hazards and its monitoring using remote sensing (Richardson and Reynolds 2000). Several studies have concluded that remotely sensed data is time and cost-effective geo-spatial technique for glacial lake monitoring, development of glacial lake inventory and identification of potential glacial lakes in order to prepare GLOF risk reduction plan (Quincey et al. 2005). Many factors can lead to the breaching of glacial lakes particularly location of lake, stability of slope, seismicity of the area, frequency and magnitude of rock or ice avalanches (Quincey et al. 2007).

The GLOFs pose serious risk to human life, their property and infrastructure (Westoby et al. 2014). In these circumstances, water may leak through sub-glacial tunnels, along the ice edge separating the glacier from the valley side, or by the ice dam breaking mechanically (Clague and Evans 2000). Consequently, a number of studies have adopted an empirical approach to volume calculation from satellite imagery based on known relationships between lake depths, areas and volumes. This allows rapid and simple calculation of lake volumes from widely available satellite imagery, whilst avoiding the necessity for often challenging fieldwork (O'Connor et al. 2001). Therefore, the aim of this study is to assess GLOF hazard and map the elements at risk located in the downstream area. The results of this study can assist decision makers for effective policy formulation that will reduce the risk of GLOFs and enhance community resilience.

2. Materials and Methods

2.1. Study Area

Geographically, Hunza-Nagar valley is situated in Gilgit Baltistan, Northern Pakistan. This study area is located at the altitude of 3000m above mean sea level and extends from 76°0′45.354″E longitude to 73°59′26.466″E longitude and 36°51′38.359″N latitude to 35°55′22.231″N latitude (Afsar et al. 2013). Relatively, shares borders with Afghanistan and China on the northwest and northeast, respectively, and with District Gilgit on the southwest (Fig. 1). This area is distinguished geologically by various rock combinations. This area is known as paradise on Earth and is situated in an area of active tectonics brought on by the collision of the Indian and Eurasian plates (Rehman et al. 2021). It also features a variety of tourist attractions, mineral deposits, and natural resources. The total area of these districts was 14,305.08 km^2. The main tributary of Pakistan's longest river, the Indus, is the Hunza-Nagar River. Around 96% of households in Hunza and Nagar have access to agricultural land and estimate both basic and monetary needs. Upstream population in the Hunza and Nagar sub-basin in the Indus basin relies primarily on natural resources (Dilshad et al. 2019).

2.2. Research Metodology

This study is based on secondary data. Shuttle Radar Topographic Mission (SRTM) Digital Elevation Model (DEM) was downloaded from USGS open source geo-database. Vector data including road network, human settlements and drainage network were digitized in ArcGIS 10.5 by utilizing Google Earth image as base map. The output spatial layers were overlaid on to map the elements exposed to GLOF (Fig. 2).

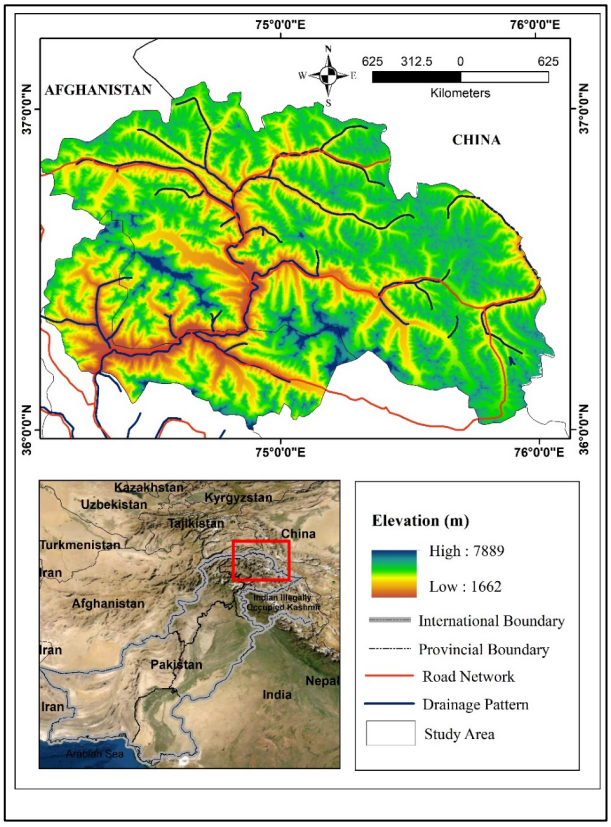

Figure 1. Location of Study Area

2.2.1. Lake Area and Volume Estimation

Area of lake was calculated from the vector mapping of lakes. The years taken were 2016, 2018 and 2020. Five glacial lakes from study region were delineated from Google Earth and further calculation for volume has been done. Although bathymetric survey is considered to be the most accurate method in case of lake volume estimation, but an empirical equation established by Huggel (Huggel et al. 2002) was used in this study. This method has been widely used by many researchers to overcome lack of field data which is hard to collect. Volume of the glacial lake in m^3 is calculated using in Equation (1).

$$V = 0.104A^{1.42} \quad (1)$$

Where "V" is volume of the glacial lake and "A" is area in m^2. The above relationship has been used to estimate the volume and further calculation of maximum discharge in potential lake is calculated by using Equations II and III.

$$PE = 9800 \times h \times V \quad (2)$$

$$Q_{max} = 0.00013 \times PE^{0.6} \quad (3)$$

Where "h" = Height of the moraine dam, "PE" = Potential Energy of the lake, Qmax = Maximum probable flow.

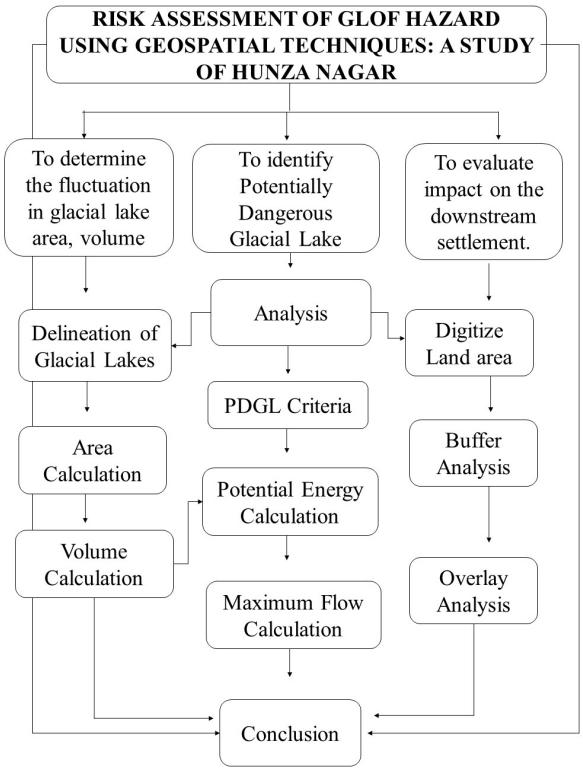

Figure 2. Research design

2.2.2. Identification of Potential Glacial Lakes

The potentially dangerous glacial lakes were identified by utilizing the well-established four parameters including lake area should be greater than 0.500m², lake should be attached or in the proximity of parent glacier, supra-glacial lakes should be around them and lakes should have steep slopes (Bairacharya et al. 2007; Mool et al. 2011; Ashraf et al. 2012).

2.2.3. Mapping of Element at Risk

In downstream areas, elements at risk were identified in 500m buffer zone and goe-visualized by overlapping the spatial layers of elements at risk on SRTM DEM. The elements at risk were human settlements, agricultural land and crop, and roads. The results were presented in the form of maps, tables and graphs.

3. Results

This study carried out area mapping around the lakes, downstream hazard vulnerability risk assessment. Bathometry of the lake using Remote Sensing and empirical formula respectively to determine the lake's development processes and assess the prospect of the GLOF from the lake. The surface area and volume of the lake in 2016, 2018 and 2020 are given in the Table 1. Graphs of area and volume are shown in Fig. 3 and Fig. 4. The detailed surface area mapping of glacial lakes is shown in Fig. 5.

Table 1. Area and Volume of Glacial Lakes

Sr. No.	Name	Area (m²)			Volume (m³)		
		2016	2018	2020	2016	2018	2020
1	Kacheli Lake	4211	2128	3362	14576.7391	5530.35544	10579.15
2	Rush Lake	54068	41578	56522	546774.903	376547.392	581850.8
3	Passu Lake	69962	76373	52696	788383.79	892910.494	526771.3
4	Borit Lake	161869	142726	134999	2594452.78	2169840.11	2003378
5	Batura Lake	29788	316754	34597	234515.769	6730676.74	289830.3

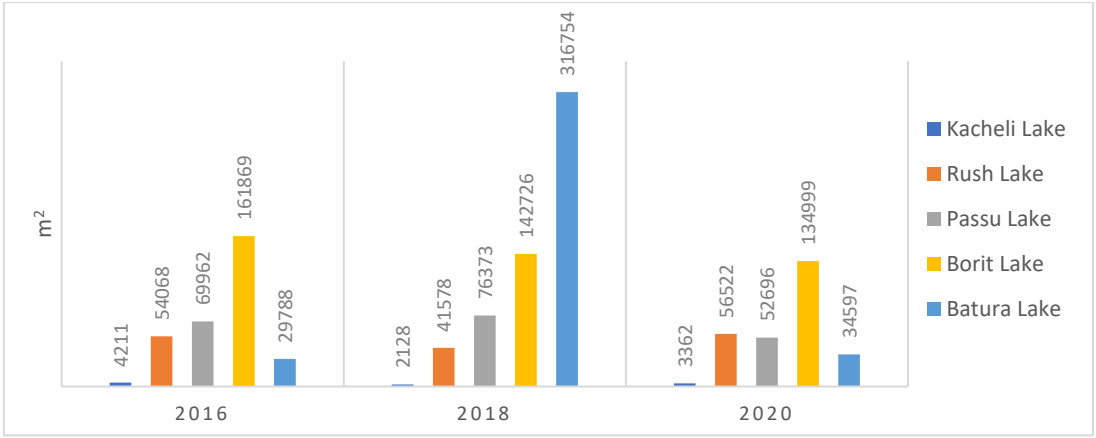

Figure 3. Variation in Area of Glacial Lakes (2016-2020)

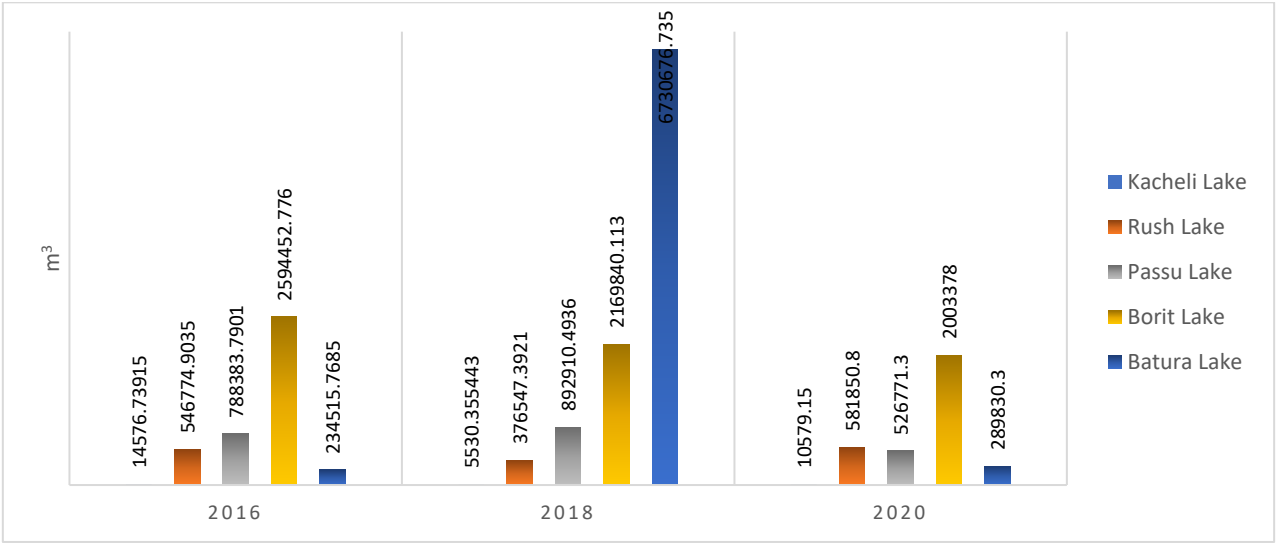

Figure 4. Variation in Volume of Glacial Lakes (2016-2020)

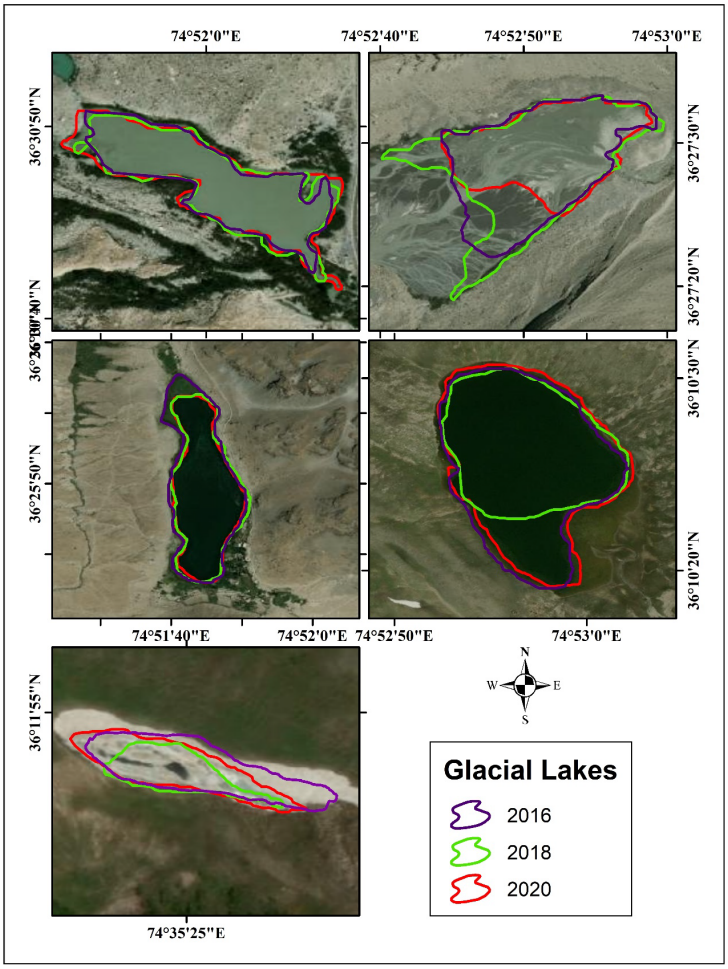

Figure 5. Suface Area mapping of selected lakes (a) Batura Lake, (b) Passu Lake, (c) Borit Lake, (d) Rush Lake, (e) Kacheli Lake

3.1. Potential Glacial Lakes

According to the aforementioned criteria, Passu Lake is only lake that fulfil all the requirements of PDGL. The area of Passu Lake is greater than 0.500 m in all selected years. It is close and connected to the snout of parent glacier i.e. Passu Glacier that is continuously feeding the lake. For the third criterion, it directly falls in Hunza River and major infrastructure and settlement is present in its downstream area. The slope over the area is steep enough to start a major event (Fig. 6).

In 2020, the volume of Passu lake was 526771.3m^3 and the maximum discharge Q_{max} can be upto 869.57 m^3/s if it outburst 100%. If the lake outburst 25% then the maximum discharge will be 217.39 m^3/s. If the lake outburst 50% then the maximum discharge will be 434.79 m^3/s. If the lake outburst 75% then the maximum discharge will be 652.18 m^3/s (Table 2).

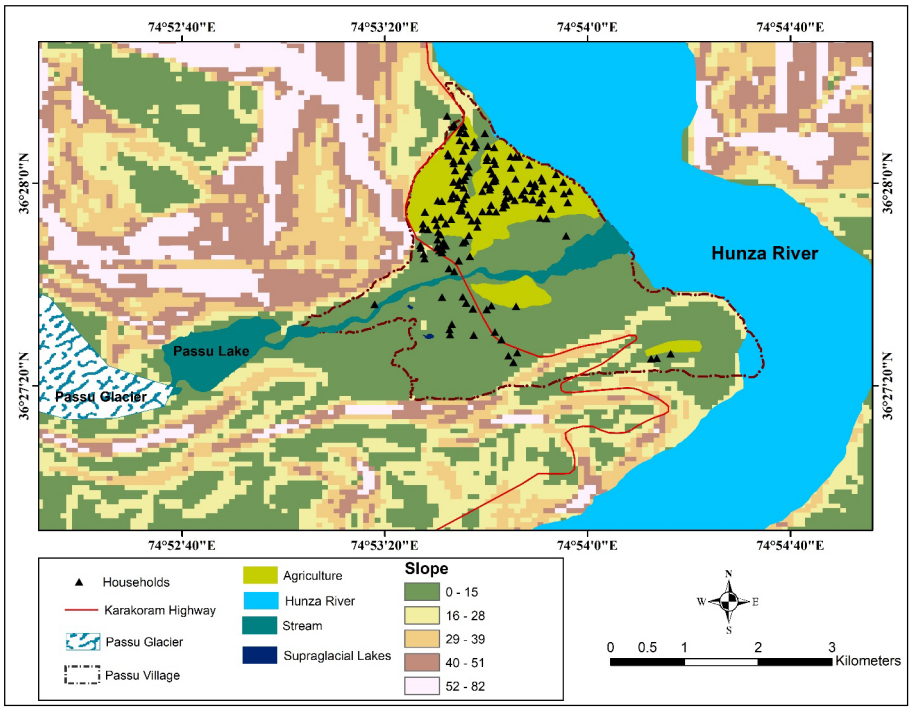

Figure 6. Passu Lake and Elements at Risk in Downstream Area

Table 2. Percentage of Discharge in Passu Lake

% age of discharge	Total Discharge in 2020 (m^3/s)
25%	217.39
50%	434.79
75%	652.18
100%	869.57

3.2. Mapping of Potential Areas at Risk

Hazard map was developed by overlaying spatial layers of element at risk, land cover, and 500m buffer zone on slope of the area (Fig. 7). Segments of Karakoram highway are within hazard zones and around 100 houses. The Passu lake outburst in will directly increase the volume of Hunza River and it will eventually cause flooding in downstream areas of Hunza River. Almost 10 villages are exposed to floods in Hunza River.

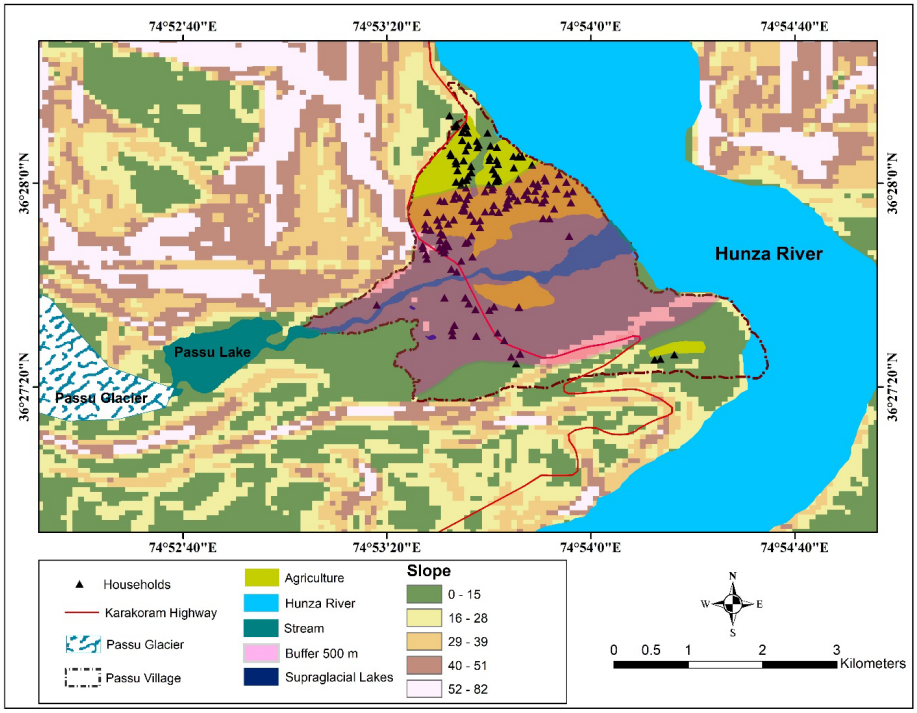

Figure 7. Hazard Zones in Passu Village

4. Discussion

Analysis revealed that geo-spatial techniques are time and cost effective in comparison to filed surveys. In this study, SRTM DEM and Google Earth image has been utilized to identify potential glacial lakes and analyze the volume of lakes by applying vector analysis. Hazard map is prepared depicting elements at risk. A bridge on the Karakoram Highway (KKH) and numerous houses in the Passu village, which is located on the right bank of the Hunza River, were destroyed by at least two outbursts of the 38 km long, east-west oriented Passu Glacier in the past 20 years. Even though the Passu Lake has natural drainage and it seems unlikely that it will erupt, it did so inexplicably, suffering enormous losses. Investigations revealed that a significant amount of water was once stored beneath the glacier's broken tongue, and that under normal circumstances, this water still discharges to the adjacent lake. During the past outburst events, very heavy loads of mud as well as debris flowed downstream under the action of gravity flow destroying the structures on the way (Muneeb et al. 2021).

Analysis further revealed that Passu is potentially dangerous lake in Hunza basin (Qureshi et al. 2022; Rasul et al. 2011). Similarly, out of 5 lakes, Passu is considered to be the most dangerous one in this study. Saifullah et al. states that Passu glacial retreat that increases the flow of water in 2016 and the area and volume increase as compared to past years (Saifullah et al. 2020). These results can also be noticed in this study as the volume in 2016 is higher than 2020, glacial surge could be the reason of decreasing volume in 2020. Anwar and Iqbal shows that the area of Passu glacier is lowest in 2017 from past 23 years that will eventually increase the volume of Passu Lake in those years, this can clearly be seen in this study that the area and volume of Passu in 2018 in highest (Anwar and Iqbal 2018). It is highly recommended to monitor expanding lakes. Traditional surveys find it very challenging to monitor these lakes because of their remote locations and high altitudes (Mool 1995). Sensor based automatic weather stations and Hydro-gauging stations are highly recommended to provide real-time data. This will help in decision making and issuance of early warning. Timely early warning can reduce the chances of potential damages particularly human life.

Furthermore, breaching of glacial lake leads to GLOFs that pose a significant threat to life and infrastructure (Richardson et al. 2000; Westoby et al. 2014). Other potentially dangerous lakes are dammed by ice, either in ice-marginal locations where surface meltwater or water from tributary valleys ponds against the glacier margin or where advancing (often surging) glaciers block river drainage like Kyagar Glacier (Haemmig et al. 2014). In these situations, water may escape through sub-glacial tunnels, along the ice margin between the glacier and valley side or by mechanical failure of the ice dam (Mayer and Schuler 2005; Ives et al. 2010; Aslam et al. 2022).

In short, further research on GLOF risk perception and utilization of high-resolution satellite images and field work is recommended for better results. The results of such studies can assist decision makers for effective policy formulation that will reduce the risk of GLOFs and enhance community resilience against GLOFs.

5. Conclusion

The study concludes that Passu Lake is the most impactful lake for future GLOF hazards in the region. The volume of the lake was 788383.79 m^3 in 2016 that increases to 892910.494 m^3 in 2018 and then decrease to 526771.3 m^3 in 2020. This decrease is due to the instability of parent glacier which is a common phenomenon observed in Karakoram (Karakoram Anomaly). Buffer zone shows 500 m areas most vulnerable that includes agriculture, settlements, and infrastructure. Some settlements along the Hunza River downstream from Passu Lake and stretches of the Karakoram Highway are among the risk regions. These components could sustain harm from any upcoming GLOF event brought on by the Passu Lake outburst. The results of this study will be beneficial in minimizing the negative effects of future GLOF events in the Passu sub-watershed and will be helpful in creating early warning systems in the vulnerable areas. All aspects of disaster management, including mitigation, readiness, response, and recovery, involve hazard and risk maps. The use of hazard and risk maps can help avoid severe events from turning into disasters, but they cannot stop a catastrophic phenomenon from occurring. Even though it is often difficult to prevent natural disasters like GLOFs, having understanding of their nature and potential scope can help DM authorities prepare for and respond to emergency situations and disasters. The effects of these catastrophes are also mitigated by increased preparedness.

It is also concluded form the study that further research on GLOF risk perception is recommended. Utilization of high resolution satellite images and field work is also recommended. The results of this study can assist decision makers for effective policy formulation that will reduce the risk of GLOFs and enhance community resilience against GLOFs.

References

Afsar, S., Abbas, N., & Jan, B. (2013). Comparative study of temperature and rainfall fluctuation in Hunza-nagar District. Journal of Basic & Applied Sciences, 9, 151-156.

Anwar, Y., & Iqbal, J. (2018). Spatio Temporal Change Of Selected Glaciers Along Karakoram Highway From 1994–2017 Using Remote Sensing and GIS Techniques. ISPRS annals of the photogrammetry, remote sensing and spatial information sciences, 4, 7-11.

Ashraf, A., Naz, R., & Roohi, R. (2012). Glacial lake outburst flood hazards in Hindukush, Karakoram and Himalayan Ranges of Pakistan: implications and risk analysis. Geomatics, Natural Hazards and Risk, 3(2), 113-132.

Aslam, A. B., Rana, I. A., Shah, S. S., & Mohuddin, G. (2022). Climate change and glacial lake outburst flood (GLOF) risk perceptions: An empirical study of Ghizer District, Gilgit-Baltistan Pakistan.

International Journal of Disaster Risk Reduction, 83, 103392.

Bajracharya, S. R., Mool, P. K., & Shrestha, B. R. (2007). Impact of climate change on Himalayan glaciers and glacial lakes: case studies on GLOF and associated hazards in Nepal and Bhutan. International Centre for Integrated Mountain Development (ICIMOD).

Bolch, T., Buchroithner, M. F., Peters, J., Baessler, M., & Bajracharya, S. (2008). Identification of glacier motion and potentially dangerous glacial lakes in the Mt. Everest region/Nepal using spaceborne imagery. Natural Hazards and Earth System Sciences, 8(6), 1329-1340.

Clague, J. J., & Evans, S. G. (2000). A review of catastrophic drainage of moraine-dammed lakes in British Columbia. Quaternary Science Reviews, 19(17-18), 1763-1783.

Dilshad, T., Mallick, D., Udas, P. B., Goodrich, C. G., Prakash, A., Gorti, G., ... & Rahman, A. (2019). Growing social vulnerability in the river basins: Evidence from the Hindu Kush Himalaya (HKH) Region. Environmental Development, 31, 19-33.

Haemmig, C., Huss, M., Keusen, H., Hess, J., Wegmüller, U., Ao, Z., & Kulubayi, W. (2014). Hazard assessment of glacial lake outburst floods from Kyagar glacier, Karakoram mountains, China. Annals of Glaciology, 55(66), 34-44.

Huggel, C., Kääb, A., Haeberli, W., Teysseire, P., & Paul, F. (2002). Remote sensing based assessment of hazards from glacier lake outbursts: a case study in the Swiss Alps. Canadian Geotechnical Journal, 39(2), 316-330.

Ives, J. D., Shrestha, R. B., & Mool, P. K. (2010). Formation of glacial lakes in the Hindu Kush-Himalayas and GLOF risk assessment (pp. 10-11). Kathmandu: ICIMOD.

Mayer, C., & Schuler, T. V. (2005). Breaching of an ice dam at Qorlortossup tasia, south Greenland. Annals of Glaciology, 42, 297-302.

Mernild, S. H., Beckerman, A. P., Yde, J. C., Hanna, E., Malmros, J. K., Wilson, R., & Zemp, M. (2015). Mass loss and imbalance of glaciers along the Andes Cordillera to the sub-Antarctic islands. Global and Planetary Change, 133, 109-119.

Mool, K. P. (1995). Glacier lake outburst floods in Nepal. J. Nepal Geological Society, Kathmandu, 11, 273-280.

Mool, P. K., Maskey, P. R., Koirala, A., Joshi, S. P., Lizong, W., Shrestha, A. B., ... & Shrestha, R. B. (2011). Glacial lakes and glacial lake outburst floods in Nepal.

Muneeb, F., Baig, S. U., Khan, J. A., & Khokhar, M. F. (2021). Inventory and GLOF susceptibility of glacial lakes in Hunza River Basin, Western Karakorum. Remote Sensing, 13(9), 1794.

O'Connor, J. E., Hardison, J. H., & Costa, J. E. (2001). Debris flows from failures of Neoglacial-age moraine dams in the Three Sisters and Mount Jefferson Wilderness areas, Oregon (No. 1606). US Geological Survey.

Pinglot, J. F., Pourchet, M., Lefauconnier, B., Hagen, J. O., Vaikmäe, R., Punning, J. M., ... & Kameda, T. (1994). Natural and artificial radioactivity in the Svalbard glaciers. Journal of environmental radioactivity, 25(1-2), 161-176.

Quincey, D. J., Lucas, R. M., Richardson, S. D., Glasser, N. F., Hambrey, M. J., & Reynolds, J. M. (2005). Optical remote sensing techniques in high-mountain environments: application to glacial hazards. Progress in Physical Geography, 29(4), 475-505.

Quincey, D. J., Richardson, S. D., Luckman, A., Lucas, R. M., Reynolds, J. M., Hambrey, M. J., & Glasser, N. F. (2007). Early recognition of glacial lake hazards in the Himalaya using remote sensing datasets. Global and Planetary Change, 56(1-2), 137-152.

Qureshi, J. A., Khan, G., Ali, N., Ali, S., ur Rehman, S., Bano, R., ... & Ehsan, M. A. (2022). Spatio-temporal Change of Glacier Surging and Glacier-dammed Lake Formation in Karakoram Pakistan. Earth Systems and Environment, 1-14.

Rasul, G., Chaudhry, Q. Z., Mahmood, A., Hyder, K. W., & Dahe, Q. (2011). Glaciers and glacial lakes under changing climate in Pakistan. Pakistan Journal of Meteorology, 8(15).

Rehman, Q. U., Ahmed, W., Waseem, M., Khan, S., Farid, A., & Shah, S. H. A. (2021). Geophysical investigations of a potential landslide area in Mayoon, Hunza District, Gilgit-Baltistan, Pakistan. Rudarsko-geološko-naftni zbornik, 36(3).

Richardson, S. D., & Reynolds, J. M. (2000). An overview of glacial hazards in the Himalayas. Quaternary International, 65, 31-47.

Saifullah, M., Liu, S., Adnan, M., Ashraf, M., Zaman, M., Hashim, S., & Muhammad, S. (2020). Risks of glaciers lakes outburst flood along China Pakistan economic corridor. In Glaciers and the Polar Environment. IntechOpen.

Westoby, M. J., Glasser, N. F., Brasington, J., Hambrey, M. J., Quincey, D. J., & Reynolds, J. M. (2014). Modelling outburst floods from moraine-dammed glacial lakes. Earth-Science Reviews, 134, 137-159.

Advanced Geomatics

http://publish.mersin.edu.tr/index.php/geomatics/index

e-ISSN: 2791-8637

Landslide Risk Assessment using Geo-spatial Technique: A study of District Abbottabad, Khyber Pakhtunkhwa, Pakistan

Anum Gull[1], Anum Liaqut[1], Shakeel Mahmood *[1]

*[1] Department of Geography, Government College University Lahore, 54000, Lahore, Pakistan; (*anumg977@gmail.com*; Anummughal005@gmail.com; shakeelmahmoodkhan@gmail.com)*

Keywords

Landslides,
Risk,
GIS,
Remote Sensing,
Weighted overlay,
Zonation.

Research Article

Received : 07.04.2023
Revised : 08.08.2023
Accepted : 12.09.2023
Published : 30.09.2023

* **Corresponding Author**
shakeelmahmoodkhan@gmail.com

Abstract

The study focused on identifying the causes and landslide-prone areas in Abbottabad District of Northern Pakistan. Remote sensing data, including NASA's Shuttle Radar Topographic Mission's (SRTM) Digital Elevation Model (DEM) and Landslide-8 imagery, were used in combination with geographic indices to identify the factors of landslides, such as slope, aspect, elevation, vegetation cover, hydrology, SAVI, and land cover change. The weighted overlay technique was used to assign weights to map layers and find the risk zones in the study area. The study revealed that the region is at risk of landslides due to high rock, sloppy areas, and built-up expansion. The major cluster of landslide risk is in the western and southern parts of the region, which are also more populated. The results and landslide susceptibility maps can be used to better understand the existence of landslides and for mitigation purposes, but field surveys are necessary for better predictions. Overall, the study provides valuable information for relevant authorities to prioritize landslide mitigation efforts in the region.

1. Introduction

Landslides can have devastating effects on both the natural environment and human settlements (El-Rabbany, 2016). They can result in loss of life and property damage, disrupt transportation and communication networks, and cause long-term environmental damage (Lynn, 2006). Therefore, it is important to understand the factors that contribute to landslides and to develop strategies to mitigate their impact (Schuster et al., 1986; Phillips et al. 2021). In addition to deforestation and excessive water, other factors that contribute to landslides include steep slope angles, weak or unstable rock or soil, seismic activity, human activities such as construction or mining, and natural processes such as erosion and weathering (McColl ,2022; Jindal et al. 2023). Landslides can also be triggered by a combination of factors, such as heavy rainfall following a period of drought (Shi Min, 2015).

There are several methods for predicting and mitigating landslides, including geological mapping, slope stabilization techniques, and early warning systems (Ju et al. 2020). Prevention strategies can include maintaining natural vegetation cover, controlling erosion, limiting development in high-risk areas, and implementing appropriate land-use planning and zoning regulations (Javed, 2019; Cherkez et al. 2021). The use of GIS and RS in landslide risk assessment and management has become increasingly common in recent years, as these tools provide a powerful means of analyzing large volumes of spatial data and identifying areas at high risk of landslides (Conners, 2019; Deaana, 2019; Thigale, 2006; Tarun, 2019; Sonia, 2017)). Remote sensing data from satellites such as Landsat 8 can be used to generate high-resolution imagery and elevation data, while GIS software can be used to process and analyze this data to identify potential landslide risk factors such as slope,

Cite this;

Gull, A., Liaqut, A. & Mahmood, S. (2023). Landslide Risk Assessment using Geo-spatial Technique: A study of District Abbottabad, Khyber Pakhtunkhwa, Pakistan. Advanced Geomatics, 3(2), 47-55.

aspect, soil type, and land use (Dai and Lee, 2001). Various statistical models have also been developed to predict landslide occurrence based on these risk factors, including logistic regression, artificial neural networks, and fuzzy logic. These models can be used to generate landslide susceptibility maps, which can be used by local authorities to inform decision-making and policy planning efforts related to disaster management (Clerici et al., 2002; Akgun and Serhat, 2008).

The northern area of Pakistan, with its rough terrain, heavy rainfall, and seismic activity, is particularly susceptible to landslides, which can have significant impacts on the local economy and society. Therefore, it is essential to identify areas at high risk of landslides and take appropriate mitigation measures to reduce the potential impacts. Landslides are a significant geological hazard in mountainous regions, and their occurrence is influenced by a variety of factors. It is important to understand and address these factors to minimize the impact of landslides on both the natural environment and human settlements (Akbar, 2011). This aims to assess landslide risk in the study region using GIS indices and other causative factors. The resulting landslide susceptibility map will be a valuable resource for local government authorities to help inform their decision-making and policy planning efforts related to disaster management in the region. Overall, the use of GIS and RS in landslide risk assessment and management is an important tool for reducing the potential impacts of landslides on human settlements and infrastructure.

2. Materials and Methods

2.1. Study Area

Abbottabad District has been selected as study area that lies between latitude of 34°10'7.5"N and a longitude of 73°13'17.39"E in Khyber Pakhtunkhwa (Figure 1). This district is dominated by the mountains and hills and Kunhar and Jhelum rivers enters Abbottabad District from the North so that center of region is still marshy (SEMDA, Abbottabad Development Authority). The climate of Abbottabad is temperate with an average minimum temperature 0.5°C and maximum temperature 13.2°C. (PMD, 2019). This region has been frequently or severely affected by the land sliding due to moderately soil erosion as a result of heavy snowfall and frequent rains.

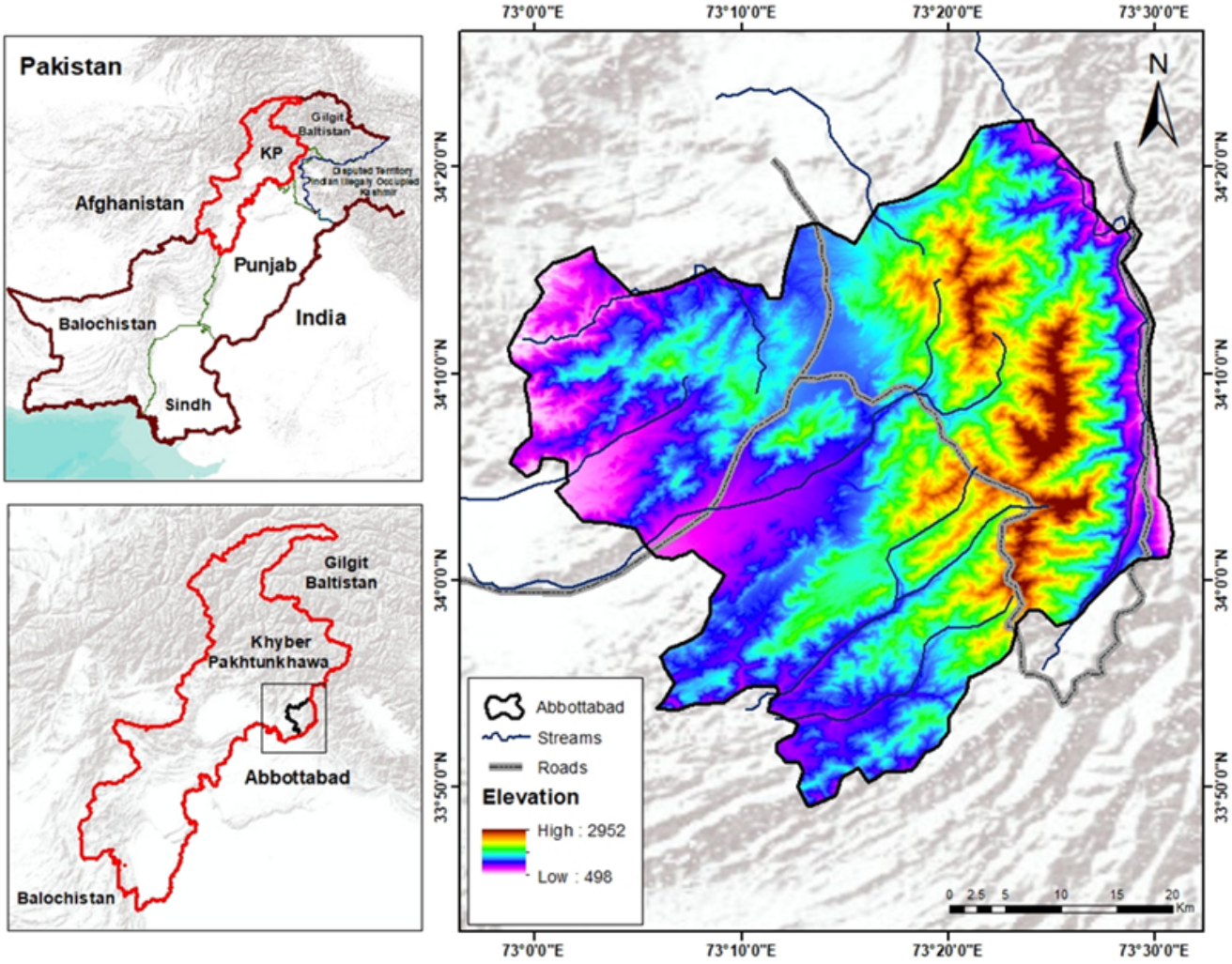

Figure 1. The experimantal setup.

2.2. Data Sources

The selected input parameters for landslide risk assessment were elevation, slope and aspect. The spatial layers of these parameters were extracted from Shuttle Radar Topography Mission (SRTM) based DEM having 30m spatial resolution. As suggested by Lee et al. (2004), Geological structures and formations also influence the genesis of landslide, were digitized using Geological map acquired from Geological Survey of Pakistan (GPS). Satellite images of Landsat 8 (06 July, 2022) were acquired from Earth Explorer open source geo-database. Supervised image classification was applied to extract the land cover classes as suggested by Siraj et al. (2023) and Saleem and Mahmood (2023).

Normalized difference water index (NDWI), Normalized difference vegetation index (NDVI) and Soil adjusted vegetation index (SAVI) were combined in GIS environment to form landslide catalog to carry out landslide hazard assessment after (Nefeslioglu et al., 2008). The most commonly used indices are NDVI is used for vegetation cover density (Javed, 2007). The NDWI is used to determine the presence of moisture in soil cover. Higher NDWI values indicate sufficient moisture, while a low value indicates water stress (Javed, 2019). SAVI is used in the adjustment of the Normalized Difference Vegetation Index to correct for the effect of soil intensity when vegetative cover is little (Clerici et al., 2002). Variations in land cover control the spatial distribution of landslides along with other conditioning parameters (Malek et al., 2015).

Generally, vegetation tends to resist the erosion process whereas bare rock or soil is more susceptible to slope failure. Slope angle is an important geomorphic factor responsible for initiation of slope movements, to be considered for preparation of landslide susceptibility maps. Steep slopes are more susceptible to failure as compared to gentle ones. The Abbottabad district demonstrates variation in topography ranging from steep to gentle slopes, high plains to narrow gorges and high cliffs (Evans, 1980). Therefore, slope, aspect, geological map and different calculated indices of the study area were required to prepare risk map.

2.3. Landslide Hazard Zonation

Weighted overlay analysis is a common technique used in GIS (Geographic Information Systems) to combine and analyze multiple spatial datasets. In this approach, different layers or indices are assigned weights based on their relative importance or contribution to the final output. The weighted sum raster is then generated by adding up the weighted values of each layer at each location in the study area. This approach allows for the integration of different factors or variables that may influence a hazard or risk and helps to identify areas that are more susceptible or vulnerable to the hazard.

For creating landslide hazard map using a weighted overlay analysis approach was applied. The different indices such as NDVI, NDWI, SAVI, land use/land change, slope, and aspect were used to classify and assign weights to them based on their importance (Table 1). The weights were then used in the weighted overlay analysis to create a susceptibility map. The final weighted sum raster was created using the weighted sum overlay tool, and the raster was then divided into five different hazard zones using the equal interval method based on judgment.

Table 1. Factors Ranks

Sr No.	Factors	Ranks
1	Slope	20
2	Aspect	10
3	Elevation	10
4	Land Cover	20
5	Normalized Difference Vegetation Index (NDVI)	10
6	Normalized Difference Water Index (NDWI)	20
7	Soil Adjusted Vegetation Index (SAVI)	10

3. Results and Discussion

It is important to identify potential landslide-prone areas in advance in order to reduce the damage caused by this natural hazard. To prepare a landslide hazard zonation map, all the major factors that play a vital role in landsliding should be taken into account. The resulting map can then be used to estimate the vulnerable area and the potential impact of any future landslide event. The detail is given in the following sections.

3.1. Causative Factors

3.1.1 Slope and Aspect

Slope and aspect play an elementary role in material flow as slope provides speed and aspect indicates the direction of that steepness. Figure 2 indicates the slope angles from 9.177 to 57.08. The highest slope angles are most favorable for landslide. Slopes with different aspects differ in solar radiation intensity, which affects a multitude of factors, including temperature difference, evaporation capacity, vegetation cover.

Map of aspect indicated the total range of the values between -1 to 359. 85 (Figure 3). The highest and lowest value that show the western and eastern zones of the region. The value of aspect shows the flow of land sliding is worst throughout the wet season.

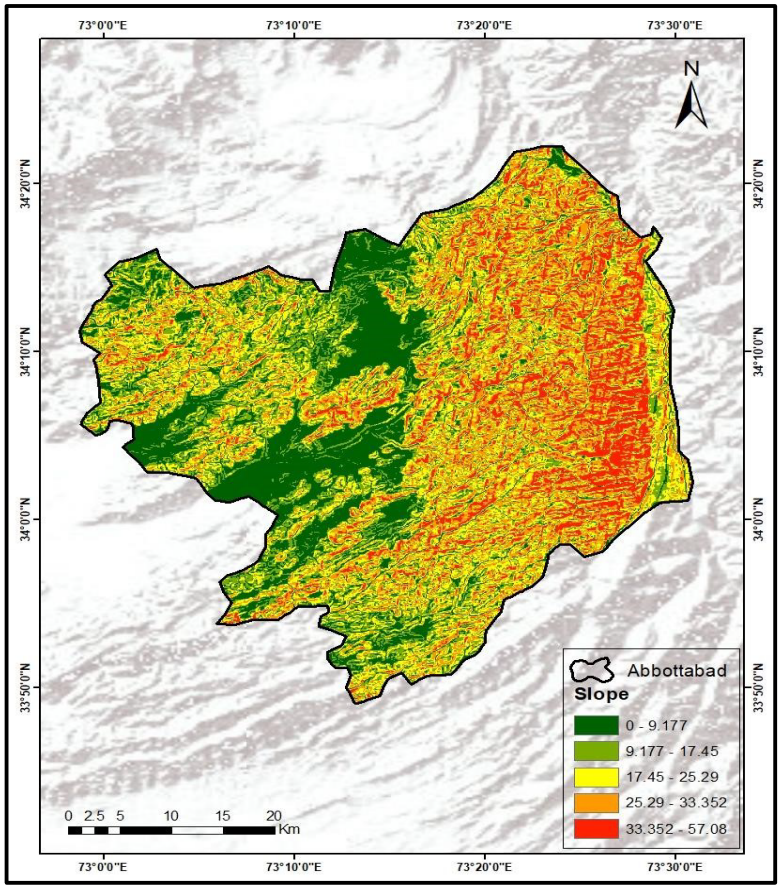

Figure 2. Slope of Abbottabad District.

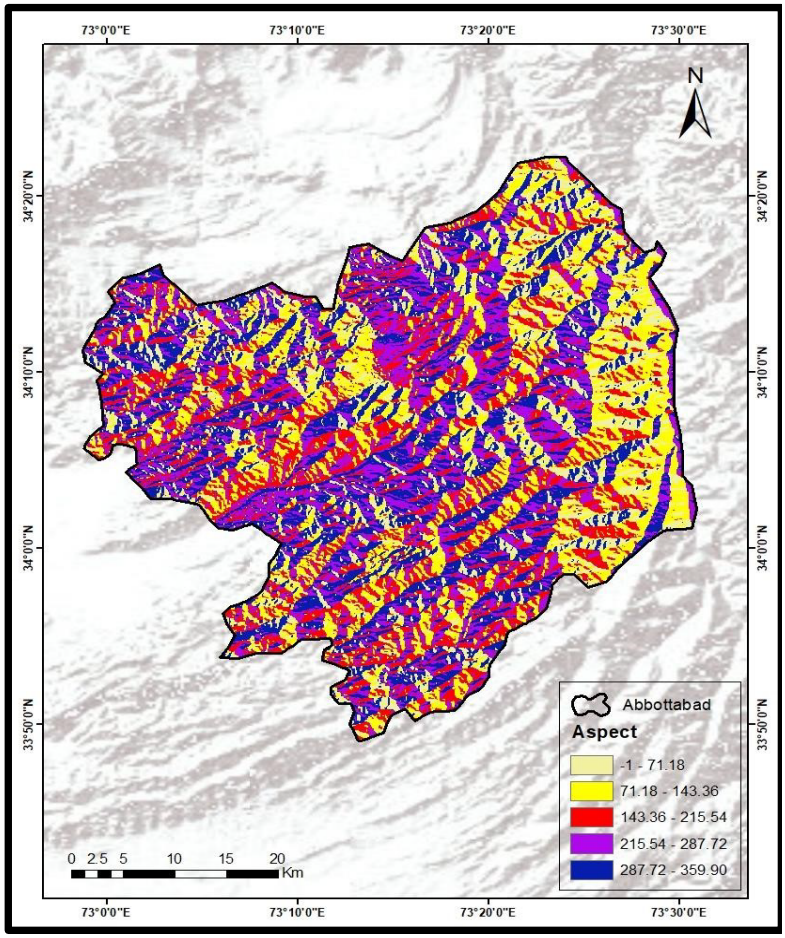

Figure 3. Aspect of Abbottabad District

3.1.2 Geology

Further, geology, is important in term of earth structure of Abbottabad district shown in Figure 4. Generally, the structure in this area are developed as a result of compression and the entire zone is part of the Lesser Himalayas. Khairabad Fault runs across the Abbottabad Block which trends in northeast-southwest direction. Mostly NE-SW trending folds are present, which have been disturbed by dip-slip faults. Stratigraphy of this region ranges from Infra Cambrian to Mio-Pliocene. The whole study area consists of different kind of sedimentary rock that is less resisting against earthquake and other earth movements. Southern side made of Paleogene and cretaceous sedimentary rock and northern side mostly comprised of meta-sedimentary rocks (Jaffery C, 2015).

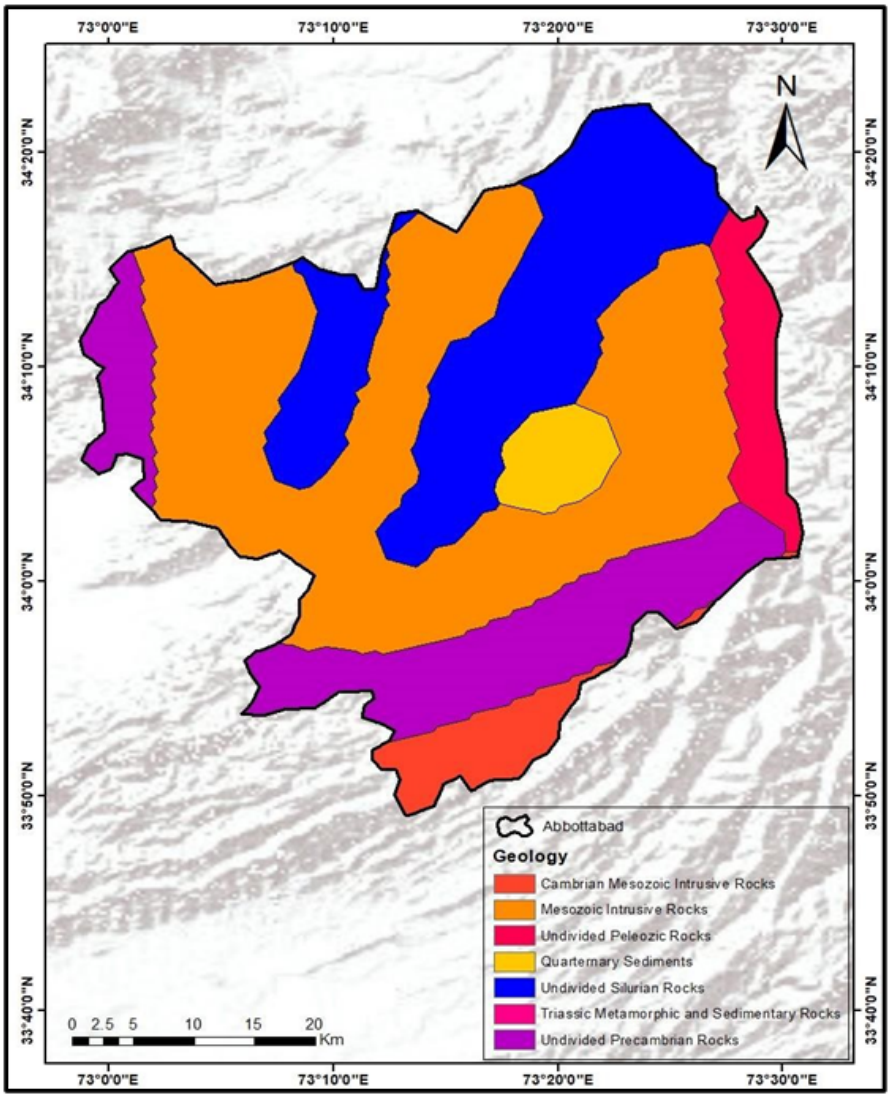

Figure 4. Geological Map of Abbottabad District

3.1.3. Indices

Figure 5 indicate the values of NDVI in the study area, there is observable change in vegetation cover the value ranges from -0.07 to 0.42. The minimum value -0.07 to 0.16 of Normalized Difference Vegetation cover was found in the northeast to southeast and central part of the study area. The probability of landslide occurrence in that part of region is relatively high as the higher values 0.42 shows the richer and healthier vegetation in region. Study area has many small tributaries and receive high rainfall in both season (summer and winter) so, in figure 6, the maximum value of NDWI 0.13 shows the higher probability of landslide occurrence in the whole region. while, minimum value -0.22 shows the low water content where the possibility of landslide occurrence is low. Figure 7 illustrates the soil brightness in the study area where vegetation low. The SAVI index is found to be a significant footstep that can refer to active soil-vegetation systems from remotely sensed data. The maximum value 0.04 shows the high intensity of soil and minimum value -0.11 shows the low intensity of soil in the region.

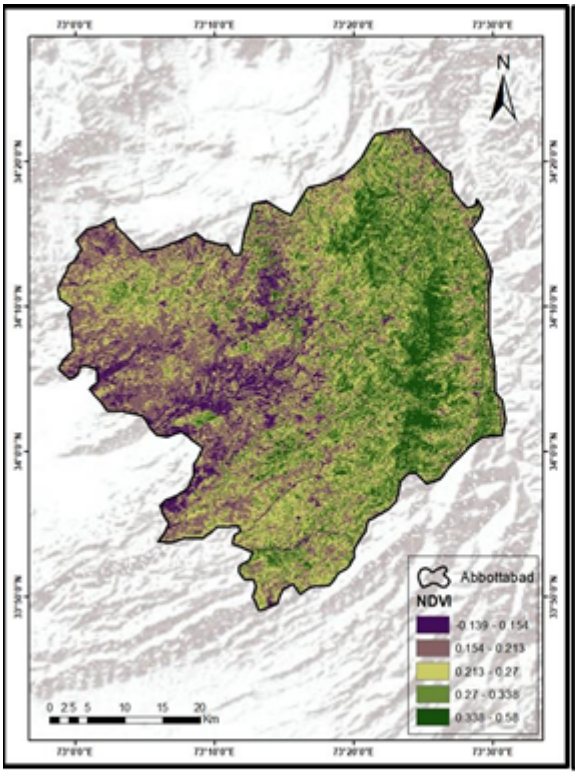

Figure 5. NDVI map of Abbottabad District

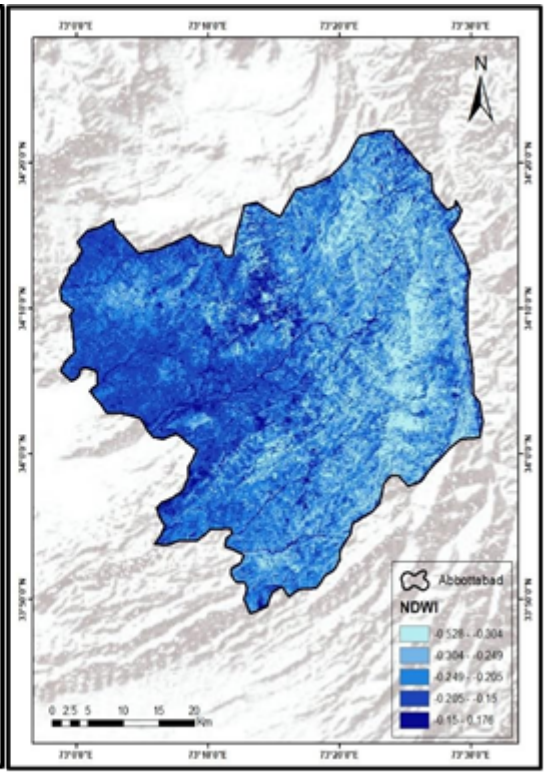

Figure 6. NDWI Map of Abbottabad District

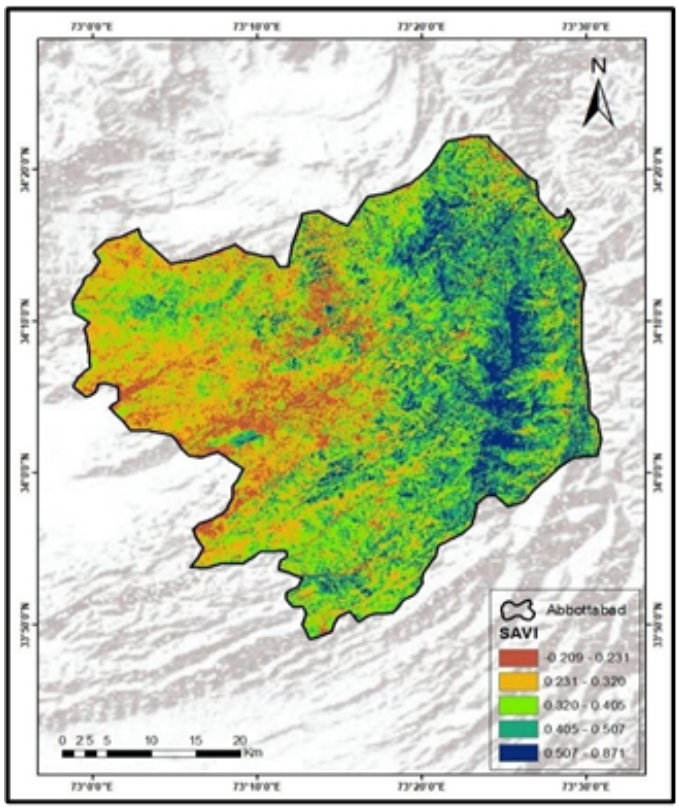

Figure 7. SAVI of the Abbottabad District

3.1.4. Land Cover

Variation in land cover control the spatial distribution of landslides along with other conditioning parameters which includes Vegetation, slope, hydrology. Changes in land cover influence the hydrological condition of slopes, leading to slope instability. Figure 8 shows the variation in Land Cover in the study area. The red shade in central part of the region indicates the built up surrounded by rocks and vegetation. The blue color in the region indicates the water and pink color shows which composed of bare Soil. Green color indicates the vegetation cover in study area.

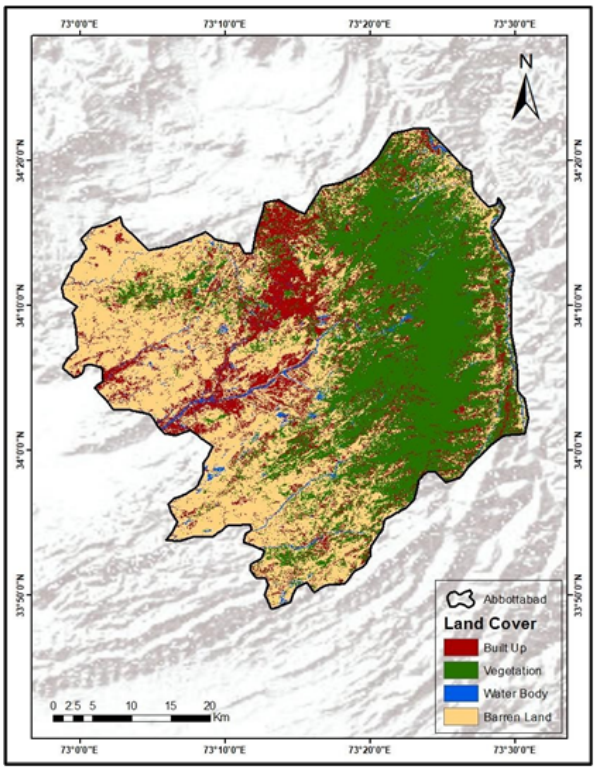

Figure 8. Land Cover of Abbottabad District

3.1.5. Risk Zonation

All above indices maps of study area were needed to mapped the final risk zonal map.

LSI (Landslide susceptibility index) in ArcGIS was a very dominant method used to allocate weight to six parameters. All were reclassified and assigned equal weights in percentages mention in table 1. The result of landslide risk zone mapping was used to detect the landslide prone areas in Abbottabad District. Figure 9 plainly show the landslide high risk areas in western part of the study region, that are the areas less vegetation, high water content and exposed soil. As far as geological structure, whole area made-up of meta-sedimentary rocks that are less resisting rocks against earth movement. The map was divided into five regions are shown in the Table 2 that show the landslide susceptibility index values (Figure 9).

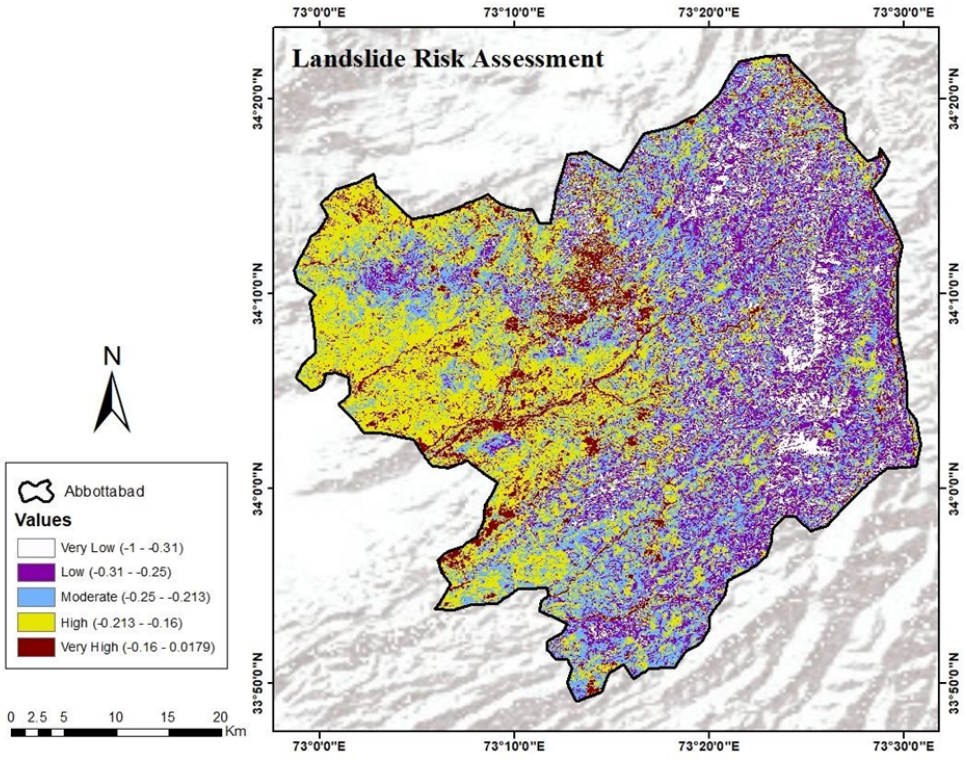

Figure 9. Landslide risk Zonation in Abbottabad District

4. Discussion

It is evident that landslides pose a significant threat to population and development in mountainous regions, particularly in developing countries like Pakistan. The unavailability of longer and precise rainfall and landslide records, along with under-reporting of landslide damages, is a significant problem in determining landslide risk in the region. However, recent studies have employed Remote Sensing and GIS techniques like the weighted overlay method to detect landslide hazard areas and create landslide risk maps.

Studies like Batool (2021) and Javed (2019) have highlighted the need for comprehensive research on various aspects of landslides in Pakistan and have provided valuable insights into the causes and consequences of landslides in the region. The use of science in risk assessment and risk management, along with embedding landslide studies within a sociopolitical framework, has resulted in a new paradigm for landslide risk assessment and management.

Creating landslide risk maps is an important step in understanding and mitigating the potential danger in specific areas. By identifying vulnerable areas, relevant authorities can prioritize mitigation efforts and take steps to protect local communities from potential landslides. During western depression and monsoon seasons, when landslides are more likely to occur, it is especially important to prioritize efforts to mitigate the risk in vulnerable areas and to ensure that local communities are relocated to safe zones. This can help to prevent loss of life and property damage caused by landslides.

In addition to the above recommendations, it is also important to establish a comprehensive landslide risk management plan for the identified vulnerable areas in Abbottabad District. This plan should involve various stakeholders, including local communities, government authorities, and disaster management departments, to ensure a coordinated effort in reducing the risk of landslides. The plan should also prioritize the implementation of measures such as slope stabilization, land-use planning, and early warning systems. Public awareness campaigns should also be conducted to educate the local communities about the risks associated with landslides and the measures they can take to reduce their vulnerability. Finally, continued research and monitoring of the landslide risk in the region is necessary to update the risk management plan and improve the accuracy of the landslide susceptibility map.

Overall, such a study is crucial for understanding the vulnerability of human lives and for taking appropriate measures to reduce the impact of landslides. By identifying potential landslide-prone areas and high-risk zones, it is possible to implement mitigation strategies that can save lives and reduce property damage in the event of a landslide.

5. Conclusion

The study's conclusion highlights the importance of understanding landslide susceptibility in order to prevent and reduce the risk of landslides. The use of GIS and thematic data layers to produce a landslide susceptibility map for the Abbottabad District provides valuable information for engineers, geologists, and land use planners to make informed decisions about future construction and development in the region. More research is needed to understand landslide effects in the region, the use of Remote Sensing and GIS techniques and the creation of landslide risk maps can aid in landslide risk assessment and management efforts in Pakistan.

The identification of the western and northwestern parts of the region as high and very high susceptible zones is particularly important for decision-making regarding future construction and development. These areas should be avoided or require careful geotechnical investigation before any development takes place.

The study's recommendation for further research on the gender distribution of the population and the type of landslide could improve the accuracy and specificity of the susceptibility map, and thus increase the effectiveness of mitigation efforts. Additionally, the study highlights the potential for early warning systems to mitigate the effects of landslides and encourages investment in mitigation efforts by society and technologists.

Author contributions

Anum Gull: Data curation, Writing-Original Draft Preparation, Validation, Control and Validation
Anum Liaqut: Conceptualization, Methodology, Software, Data curation, Writing, Visualization
Shakeel Mahmood: Investigation, Software

Conflicts of interest

There is no conflict of interest between the authors.

Statement of Research and Publication Ethics

Research and publication ethics were complied with in the study.

References

Akgun, A., Dag, S., & Bulut, F. (2008). Landslide susceptibility mapping for a landslide-prone area (Findikli, NE of Turkey) by likelihood-frequency ratio and weighted linear combination models. Environmental Geology, 54, 1127-1143.

Akgun, A., Dag, S., & Bulut, F. (2008). Landslide susceptibility mapping for a landslide-prone area (Findikli, NE of Turkey) by likelihood-frequency ratio and weighted linear combination models. Environmental Geology, 54, 1127-1143.

Bathrellos, G. D., Kalivas, D. P., & Skilodimou, H. D. (2009). GIS-based landslide susceptibility mapping models applied to natural and urban planning in Trikala, Central Greece. Estud Geol, 65(1), 49-65.

Batool, M., Ahmad, S. R., & Asif, M. (2021). An assessment of landslide hazards in Muzaffarabad-Azad Jammu & Kashmir using geospatial techniques. Pak. Geogr. Rev., 76, 164-173.

Brand, E.W., Premchitt, Y., & Phillipson, H.B. (1984). "Relationship Betweeen Rainfall and Landslides in Hong Kong." Proc. 4th Intern. Symp. On Landslides, Toronto, 1:377-384.

Cherkez, E. A., Kozlova, T. V., Shatalin, S. N., Medinets, V. I., Medinets, S. V., & Soltys, I. E. (2021, September). Landslides at the North-Western Black Sea Coast (Ukraine) and the Engineering & Geological Effectiveness of Landslide Prevention Works. In Third EAGE Workshop on Assessment of Landslide Hazards and Impact on Communities (Vol. 2021, No. 1, pp. 1-5). EAGE Publications BV.

Clerici, A., Perego, S., Tellini, C., & Vescovi, P. (2002). A procedure for landslide susceptibility zonation by the conditional analysis method. Geomorphology, 48(4), 349-364.

Crozier, M.J. (1986). "Landslides - Causes, Consequences and Environment." Croom.

Dikshit, A., Sarkar, R., Pradhan, B., Acharya, S., & Alamri, A. M. (2020). Spatial landslide risk assessment at Phuentsholing, Bhutan. Geosciences, 10(4), 131.

Ercanoglu, M., Gokceoglu, C. (2004). Use of fuzzy relations to produce landslide susceptibility map of a landslide-prone area (West Black Sea region, Turkey).

Junyi, H. (2014). Investigation on landslide susceptibility using remote sensing and GIS methods, Open Access Theses and Dissertations. 33. 5455.

Jindal, H., Yadav, A., Sehgal, A., Sharma, S., Panigrahi, A., Ranjan, D., ... & Tiwari, M. (2023). Geospatial Landslide Prediction–Analysis & Prediction From 2018-2022. Journal of Pharmaceutical Negative Results, 2589-2599.

Ju, N., Huang, J., He, C., Van Asch, T. W. J., Huang, R., Fan, X., ... & Wang, J. (2020). Landslide early warning, case studies from Southwest China. Engineering Geology, 279, 105917.

Lee, S., Choi, J., Min, K. (2004). Probabilistic landslide hazard mapping using GIS and remote sensing data at Boun, Korea. International Journal of Remote Sensing, 25 (11), 2037-2052.

McColl, S. T. (2022). Landslide causes and triggers. In Landslide Hazards, Risks, and Disasters (pp. 13-41). Elsevier.

Nefeslioglu, H. A., Duman, T. Y., & Durmaz, S. (2008). Landslide susceptibility mapping for a part of tectonic Kelkit Valley (Eastern Black Sea region of Turkey). Geomorphology, 94(3-4), 401-418.

Phillips, C., Hales, T., Smith, H., & Basher, L. (2021). Shallow landslides and vegetation at the catchment scale: A perspective. Ecological Engineering, 173, 106436.

Javed, S. (2019). Landslide hazard mapping of Bagh district in Azad Kashmir. International Journal of Economic and Environmental Geology, 47-50.

Saleem, A., & Mahmood, S. (2023). Spatio-temporal assessment of urban growth using multi-stage satellite imageries in Faisalabad, Pakistan. Advanced Remote Sensing, 3(1), 10-18.

Siraj, M., Mahmood, S., & Habib, W. (2023). Geo-spatial assessment of land cover change in District Dera Ismail Khan, Khyber Pakhtunkhwa, Pakistan. Advanced Remote Sensing, 3(1), 1-9.

Guoqing, Y., Haibo, Y., Zhizong, T., & Baosen, Z. (2011). Landslide risk analysis of Miyun Reservoir area based on RS and GIS. Procedia Environmental Sciences, 10, 2567-2573.

Advanced Geomatics

http://publish.mersin.edu.tr/index.php/geomatics/index

e-ISSN: 2791-8637

On Rational and Irrational Values of Trigonometric Functions

Veli Akarsu[*1]

[1]*Zonguldak Bülent Ecevit University, Zonguldak Vocational School, Department of Architecture and Urban Planning, 67970, Zonguldak, Türkiye; (aveli9827@gmail.com)*

Keywords

Trigonometry,
Trigonometric Functions,
Rational Number,
Irrational Number.

Research Article

Received : 20.04.2023
Revised : 08.08.2023
Accepted : 12.09.2023
Published : 30.09.2023

* **Corresponding Author**
aveli9827@gmail.com

Abstract

The beginning of trigonometry goes back 4000 years from today. Today, there are Euclidean and Non-Euclidean trigonometry. It can be said that trigonometry emerged from the need to make maps containing the position information of the stars, to determine the time and to make a calendar, mostly in astronomy. Each of the six trigonometric functions is defined according to the directed plane angle. For each angle in the domain of these functions, their values correspond to a real number consisting of rational or irrational numbers. Trigonometric functions have an important position in basic sciences and technology as well as calculations in engineering and architecture. In addition to being a branch of mathematics, trigonometry is widely used in solving geometry and analysis problems. It has an indispensable importance in engineering and architectural design and calculations. The values of trigonometric functions are usually an irrational number, with the exception of some special angle values. Irrational numbers are numbers that are not proportional. In other words, they are numbers whose results are uncertain. Examples are numbers such as pi, e, and radical. The irrational values of trigonometric functions, which are infinite decimal expansions, are given in the tables by rounding them to only four or six digits. When entering the trigonometric function values in the tables (or the values obtained in the libraries of electronic calculators) into algebraic operations, the resulting numbers are approximated. In the article, besides showing that most of the trigonometric function values such as sinθ, cosθ and tanθ of many θ angles are irrational, the effect of these functions on the result values of calculations made in engineering and architecture is interpreted.

1. Introduction

In ancient Babylon, geometry arose from the practical needs of rulers, cartographers, and builders (Britton et al. 2011). From measurements of fields, walls, posts, buildings, gardens, canals, and ziggurats (temple tower of the city god in Mesopotamia), squares, rectangles, trapezoids, and right triangles were used as the main types of practical geometric shapes (Mansfield and Wildberger, 2017). Ratio-based measurements were an important measurement in Egyptian architecture used to describe the reverse slope (cotθ) of the pyramids.

Evidence that the foundations of trigonometry date back to the ancient Babylonian period between the 19th and 16th centuries BC was reached by deciphering the Plimpton 322 (P322) tablet, the most advanced scientific work of antiquity. The P322 tablet is a trigonometric table thousands of years ahead of its time (Mansfield and Wildberger, 2017).

The table of values of modern trigonometric functions consists of rational and / or irrational ratios of trigonometric functions sinθ, cosθ and tanθ, which show the ratio of the side lengths of right triangles with hypotenuse side length, 1 unit.

The only correct trigonometric table of the world is the trigonometric table of the astronomer and mathematician Hipparchus (190-120 BC) (Mansfield and Wildberger, 2017). The pioneer of studies on trigonometry was Hipparchus, and her successor was Ptolemy (85-160 AD) (Stewart, 2009. The first person whose trigonometric table has survived is Alexandrian

Cite this;

Akarsu, V. (2023). On Rational and Irrational Values of Trigonometric Functions. Advanced Geomatics, 3(2), 56-62.

astronomer Claudius Ptolemaius (Ptolemy), who lived in the 2nd century AD (Van Brummelen, 2012). Ptolemy wrote a 13-volume book on astronomy called Mathēmatikē Syntaxis. This book has been translated into Arabic as the Almagest. In the first volume of the book, the relationship between trigonometry and astronomy was examined, and he arranged the chords ruler with the method he developed for calculating the chords of angles (Gölgeleyen ve Akarsu, 2022). He calculated the approximate value of the beam corresponding to an angle of one degree. The table of values of the sine trigonometric function is included in the book.

It can be said that the need for table of values of trigonometric functions is in astronomical observations and calendar making works rather than solving geometry problems. Each of the six trigonometric functions, consisting of three basic (sinθ, cosθ, tanθ) and three auxiliary (cscθ, secθ, cotθ) trigonometric functions, is defined according to the directed plane angle. For each angle in the domain of these functions, their values in the value set correspond to a real number consisting of rational and/or irrational numbers. The first discovered irrational number is $\sqrt{2}$. This discovery was made because of the curiosity of Greek geometers to measure the diagonal length of a square with a side length of 1 unit with a rational number. With the Pythagorean theorem, it has been proved that there is no rational number satisfying x^2=1+1=2. In the decimal notation of $\sqrt{2}$, it is followed by an infinite number of digits after the decimal symbol. Likewise, today, π has been calculated to tens of trillions of digits after the decimal point. However, the basic digits of the decimal number system used today are based on the Dedekind-Peano axioms system for natural numbers. By expanding the natural numbers axioms system, real and complex number systems are obtained. Although the decimal representation of every rational number consists of a limited number of digits, this expansion continues indefinitely for irrational numbers.

In the article, besides showing that most of the basic trigonometric function values such as sinθ, cosθ and tanθ of many θ plane angles are irrational, the effect of these values on the result values of calculations made in science is examined.

2. Method

2.1. Some trigonometric identities and equations

For plane angles α and β,

$$\begin{aligned} cos(\alpha+\beta) &= cos\alpha\,.\,cos\beta - sin\alpha\,.\,sin\beta \\ sin(\alpha+\beta) &= sin\alpha\,.\,cos\beta + cos\alpha\,.\,sin\beta \end{aligned} \quad (1)$$

$$\begin{aligned} cos(\alpha-\beta) &= cos\alpha\,.\,cos\beta + sin\alpha\,.\,sin\beta \\ sin(\alpha-\beta) &= sin\alpha\,.\,cos\beta - cos\alpha\,.\,sin\beta \end{aligned} \quad (2)$$

Matrices enable us to write them in a compact form,

$$\begin{bmatrix} cos\alpha & sin\alpha \\ -sin\alpha & cos\alpha \end{bmatrix}\begin{bmatrix} cos\beta & sin\beta \\ -sin\beta & cos\beta \end{bmatrix} = \begin{bmatrix} cos\,(\alpha+\beta) & sin\,(\alpha+\beta) \\ -sin\,(\alpha+\beta) & cos\,(\alpha+\beta \end{bmatrix} \quad (1a)$$

$$\begin{bmatrix} cos\alpha & sin\alpha \\ sin\alpha & -cos\alpha \end{bmatrix}\begin{bmatrix} cos\beta & sin\beta \\ sin\beta & -cos\beta \end{bmatrix} = \begin{bmatrix} \cos\,(\alpha-\beta) & \sin\,(\alpha-\beta) \\ \sin\,(\alpha-\beta) & \cos\,(\alpha-\beta \end{bmatrix} \quad (2a)$$

equations can be written (Beasley, 1858; Dörrie, 1950; Daut, 1951; Helton, 1972; Durell, 1975; Sigl, 1977; Barnet, 1991; Akarsu 2005; Akarsu, 2009).

Also, for any plane angle α,

$$sin^2\alpha + cos^2\alpha = 1 \quad (3)$$

the trigonometric equivalent of the Pythagorean theorem can be written.

If $\alpha = \beta = \theta$ is taken and substituted in equations (1) and (2) and equation (3) is taken into account,

$$\begin{aligned} \cos2\theta &= \cos^2\theta - \sin^2\theta = 2\cos^2\theta - 1 \\ &= 1 - 2\sin^2\theta \end{aligned} \quad (4)$$

$$\sin2\theta = 2\sin\theta\,.\,\cos\theta \quad (5)$$

equations (4) and (5) can be obtained.
Similarly, if $\beta = 2\theta$ is written in equation (1) and equations (3), (4) and (5) are taken into account,

$$\cos3\theta = 4.\cos^3\theta - 3\cos3\theta \quad (6)$$

equation (6) can also be written (Beasley,1858; Dörrie, 1950; Daut,1951; Durell, 1975).

$$\begin{aligned} sin2\theta &= 2sin\theta.cos\theta \\ sin3\theta &= 3.sin\theta.cos^2\theta\text{-}sin^3\theta \\ sin4\theta &= 4.sin\theta.cos^3\theta - 4cos\theta.sin^3\theta \\ \sin5\theta &= 5.\sin\theta - 20.sin^3\theta + 16.sin^5\theta \\ &\vdots \end{aligned} \quad (6a)$$

Or

$$\begin{aligned} sin2\theta &= 2sin\theta.cos\theta \\ sin3\theta &= 2cos\theta.sin2\theta -.sin\theta \\ sin4\theta &= 2cos\theta.sin3\theta - sin2\theta \\ \sin5\theta &= 2cos\theta.sin4\theta - sin3\theta \\ &\vdots \end{aligned} \quad (6b)$$

$$\begin{aligned} cos2\theta &= cos^2\theta - sin^2\theta = 2.cos^2\theta - 1 \\ &= 1 - 2.sin^2\theta \\ cos3\theta &= cos^3\theta - 3.cos\theta.sin^2\theta \\ cos4\theta &= cos^4\theta - 6.cos^2\theta.sin^2\theta + sin^4\theta \\ \cos5\theta &= 5.\cos\theta - 20.cos^3\theta + 16.cos^5\theta \\ &\vdots \end{aligned} \quad (6c)$$

or

$$cos2\theta = 2.cos^2\theta - 1$$
$$cos3\theta = 2cos\theta.cos2\theta - cos\theta$$
$$cos4\theta = 2cos\theta.cos3\theta - cos2\theta \quad (6d)$$
$$\cos5\theta = 2cos\theta.cos4\theta - cos3\theta$$
$$\vdots$$

$$tan2\theta = \frac{2.tan\theta}{1 - tan^2\theta}$$
$$tan3\theta = \frac{3.tan\theta - tan^3\theta}{1 - 3.tan^2\theta} \quad (6e)$$
$$tan4\theta = \frac{4.tan\theta - 4tan^3\theta}{1 - 6.tan^2\theta + tan^4\theta}$$
$$\vdots$$

or

$$tan2\theta = \frac{2.tan\theta}{1 - tan^2\theta}$$
$$tan3\theta = \frac{tan\theta + tan2\theta}{1 - tan\theta.tan2\theta} \quad (6f)$$
$$tan4\theta = \frac{tan\theta + tan3\theta}{1 - tan\theta.tan3\theta}$$
$$\vdots$$

From (6a) to (6f), different trigonometric equations can be written (Sigl, 1977).

2.2. Irrationality of Trigonometric Ratios

In this section, the irrationality of the values of the basic trigonometric functions $cos20^\circ$, $sin10^\circ$ ve $tan15^\circ$ of rational angles such as 20°, 10° ve 15° are shown.

2.2.1. Irrationality of Cos20° Trigonometric Function Value

For θ=20° let $cos60^\circ = \frac{1}{2}$ and $\cos20^\circ = x$. If these values are substituted in (6),

$$\cos60^\circ = 4.\cos^3 20^\circ - 3.\cos20^\circ$$
$$8x^3 - 6x - 1 = 0 \quad (7)$$

(7) set up the polynomial equation. Because of the way the polynomial equation (7) is set up, $\cos20^\circ$ is a root of the equation. The possible rational roots of equation (7) are $\pm1, \pm1/2, \pm1/4, \pm1/8$. If these values are substituted in equation (7), it is seen that no root satisfies equation (7).

Since none of the above 8 roots satisfy equation (7), they are not real real roots. Therefore, it is understood that equation (7) has no real roots, so $\cos20^\circ$ is an irrational number (Jung, 1962;Helton, 1972). Whether ±1,±1/(2,±1/4,±1/8) rational roots are the real roots of the equation (7) can also be understood by comparing the value of $\cos20^\circ = 0{,}939693$

Namely,

$$\cos30^\circ < \cos20^\circ < \cos0^\circ \text{ or } 0{,}866025 < \cos20^\circ < 1 \quad (8)$$

(8) inequality can be written.

2.2.2. Sin10° Displaying the Irrationality of Trigonometric

Function Value

In equation (2), β=2θ is written and equations (3), (4) and (5) are taken into account,

$$\sin3\theta = 3.\sin\theta - 4.\sin^3\theta \quad (9)$$

equation (9) can be written (Niven, 1956; Jung, 1962; Niven, 1964; Helton, 1972; Bergen, 2009; Paolillo and Vincenzi, 2021).

For $\theta = 10^\circ$, let $sin30^\circ = \frac{1}{2}$ and s $\sin10^\circ = x$. If these values are substituted in (9),

$$\sin30^\circ = 3.\sin10^\circ - 4.\sin^3 10^\circ$$
$$8x^3 - 6x + 1 = 0 \quad (10)$$

(10) polynomial equation can be established.

(4) by virtue of equality,

$$8x^3 - 6x + 1 = 0 \quad (11)$$

(11) equation is taken into account.

Let $\sin10^\circ$ be rational in equation (11). In this case, the expressions $\sin^2 10^\circ$ and $1 - 2\sin^2 10^\circ$ would also be rational. Whereas, c $\cos20^\circ$ was shown to be irrational by equation (7) and inequality (8). Therefore, it is concluded that $\sin10^\circ$ is also irrational in order not to cause a contradiction.

2.2.3. Demonstrating the Irrationality of the Tan15° Trigonometric Function Value

Starting from equation (4),

$$\tan\theta = \sqrt{\frac{1 - \cos2\theta}{1 + \cos2\theta}} \quad (12)$$

(12) can be written.

$\theta = 15^\circ$ için $cos30^\circ = \frac{\sqrt{3}}{2}$ dir. For $\theta = 15^\circ$, $cos30^\circ = \frac{\sqrt{3}}{2}$.

If these values are substituted in the equation (12);

$$tan15^\circ = \sqrt{\frac{2-\sqrt{3}}{2+\sqrt{3}}} = 0{,}2679491924.$$

Since the value of $tan15^\circ = \sqrt{\frac{2-\sqrt{3}}{2+\sqrt{3}}}$ in the square root on the right is irrational, its square root is also irrational. Hence, it is understood that the value of $tan15^\circ$ is also irrational. Hence, it is understood that the value of $tan15^\circ$ is also irrational.

3. Extending the Irrationality of Trigonometric Function Values

It can also be extended outside of some special angles, such as the indicated irrationality of the values of the trigonometric functions $Cos20^\circ$, $Sin10^\circ$ and $Tan15^\circ$. For example, trigonometric function values of angles like $62^\circ 05' 10''$ are irrational. Integer angles such as 0°, $30^\circ, 45^\circ$ and 60° and when these angles are added by 90° and its multiples, or subtracted from 90° and its multiples, all trigonometric angles The values of the functions cannot be said to be rational. But at least one trigonometric function value is rational.

For example, for all trigonometric function values of 30°,

$$\sin 30^\circ = \frac{1}{2}, \csc 30^\circ = 2 \text{ , rational; } \cos 30^\circ = \frac{\sqrt{3}}{2},$$

$$\sec 30^\circ = \frac{2}{\sqrt{3}} \text{ irrational; } \tan 30^\circ = \frac{\sqrt{3}}{3}, \cot 30^\circ = \sqrt{3}$$

irrational, It is seen that 2 trigonometric function values are rational and 4 trigonometric function values are irrational.

Starting from equation (4),

$$\cos\theta = \sqrt{\frac{1+\cos 2\theta}{2}}, \sin\theta = \sqrt{\frac{1-\cos 2\theta}{2}},$$

$$\tan\theta = \sqrt{\frac{1-\cos 2\theta}{1+\cos 2\theta}} \qquad (13)$$

(13) equations can be written. If angle θ is any angle that makes the trigonometric function value cos2θ irrational, the function values $\sin\theta = f(\cos 2\theta), \cos\theta = f(\cos 2\theta)$ can also be defined using the irrationality of cos2θ to define an infinite number of angles θ_i, $-360^\circ \leq \theta_i \leq 360^\circ$ the proof that the values of the trigonometric functions in the range of values $-1 \leq \sin\theta, \cos\theta \leq 1$ and $-\infty \leq \tan\theta \leq \infty$, are irrational can be extended. Also, this expansion can be done using the trigonometric equations (6a) to (6f).

$$sin\frac{\theta}{2} = \pm\sqrt{\frac{1-cos\theta}{2}}, cos\frac{\theta}{2} = \pm\sqrt{\frac{1+cos\theta}{2}}$$

The $\theta = 90^\circ$ angle can be taken as half of the continuous and the irrational values of the trigonometric functions can be calculated.

$$sin45^\circ = \frac{\sqrt{2}}{2}, cos45^\circ = \frac{\sqrt{2}}{2}$$

$$sin22{,}5^\circ = \frac{1}{2}\sqrt{2-\sqrt{2}}, cos22{,}5^\circ = \frac{1}{2}\sqrt{2+\sqrt{2}}$$

$$sin11{,}25^\circ = \frac{1}{2}\sqrt{2-\sqrt{2+\sqrt{2}}}$$

$$cos11{,}25^\circ = \frac{1}{2}\sqrt{2+\sqrt{2+\sqrt{2}}}$$

$$sin5{,}625^\circ = \frac{1}{2}\sqrt{2-\sqrt{2+\sqrt{2}+\sqrt{2}}}$$

$$cos5{,}625^\circ = \frac{1}{2}\sqrt{2+\sqrt{2+\sqrt{2}+\sqrt{2}}}$$

irrational values can be calculated.

Similarly, taking $\theta = \frac{90^\circ}{2^n}$, $n \epsilon \mathbb{Z}^+$, the values of the trigonometric functions of the angles are,

$$sin\frac{90^\circ}{2^n} = \frac{1}{2}\sqrt{2-\sqrt{2+\sqrt{2+\sqrt{2}+\cdots}}}$$

$$cos\frac{90^\circ}{2^n} = \frac{1}{2}\sqrt{2+\sqrt{2+\sqrt{2+\sqrt{2}+\cdots}}}$$

it can be calculated by chaining equations (Sigl, 1977).

$cos\theta = t$ olmak üzere,

$$sin\frac{\theta}{2} = \sqrt{\frac{1-t}{2}} = \frac{1}{2}\sqrt{2-2t}, cos\frac{\theta}{2} = \sqrt{\frac{1+t}{2}} = \frac{1}{2}\sqrt{2+2t}$$

$$cos\frac{\theta}{2} = \frac{1}{2}\sqrt{2+2t} = \text{k including,}$$

$$sin\frac{\theta}{4} = \frac{1}{2}\sqrt{2-2k} = \frac{1}{2}\sqrt{2-\sqrt{2+2t}}$$

$$cos\frac{\theta}{4} = \frac{1}{2}\sqrt{2+2k} = \frac{1}{2}\sqrt{2+\sqrt{2+2t}}$$

equations can be written.

$$cos\frac{\theta}{4}=\frac{1}{2}\sqrt{2+\sqrt{2+2k}}=r$$

$$sin\frac{\theta}{8}=\frac{1}{2}\sqrt{2-2r}=\frac{1}{2}\sqrt{2-\sqrt{2+\sqrt{2+2t}}}$$

$$cos\frac{\theta}{8}=\frac{1}{2}\sqrt{2+2r}=\frac{1}{2}\sqrt{2+\sqrt{2+\sqrt{2+2t}}} \quad (14)$$

$cos\theta = t$ including,

$$sin\frac{\theta}{2}=\frac{1}{2}\sqrt{2-2t}$$

$$sin\frac{\theta}{4}=\frac{1}{2}\sqrt{2-\sqrt{2+2t}}$$

$$sin\frac{\theta}{8}=\frac{1}{2}\sqrt{2-\sqrt{2+\sqrt{2+2t}}}$$

$$cos\frac{\theta}{2}=\frac{1}{2}\sqrt{2+2t}$$

$$cos\frac{\theta}{4}=\frac{1}{2}\sqrt{2+\sqrt{2+2t}} \quad (15)$$

$$cos\frac{\theta}{8}=\frac{1}{2}\sqrt{2+\sqrt{2+\sqrt{2+2t}}}$$

equations (14) and (15) can be written.

Now, using the equations (14), (15) (1) and (2), the irrationality of the sine and cosine trigonometric function values of many angles is shown below.

$$sin30^{\circ}=\tfrac{1}{2}\ ,\ cos30^{\circ}=\tfrac{1}{2}\sqrt{3}$$

$$sin15^{\circ}=\frac{1}{2}\sqrt{2-\sqrt{3}}$$

$$cos15^{\circ}=\frac{1}{2}\sqrt{2+\sqrt{3}}$$

$$sin18^{\circ}=\frac{1}{4}\ (\sqrt{5}-1)$$

$$cos18^{\circ}=\frac{1}{4}\sqrt{10+2\sqrt{5}}$$

$$sin7{,}5^{\circ}=\frac{1}{2}\sqrt{2-\sqrt{2+\sqrt{3}}}$$

$$cos7{,}5^{\circ}=\frac{1}{2}\sqrt{2+\sqrt{2+\sqrt{3}}}$$

$$sin3{,}75^{\circ}=\frac{1}{2}\sqrt{2-\sqrt{2+\sqrt{2+\sqrt{3}}}}$$

$$cos3,75^{\circ}=\frac{1}{2}\sqrt{2+\sqrt{2+\sqrt{2+\sqrt{3}}}}$$

$$sin3^{\circ}=\sin(18^{\circ}-15^{\circ})$$
$$=sin18^{\circ}cos15^{\circ}-\ cos18^{\circ}\ sin15^{\circ}$$

$$=\frac{1}{16}(\sqrt{30}+\sqrt{10}-\sqrt{6}-\sqrt{2}$$
$$-2\sqrt{20+4\sqrt{5}-10\sqrt{3}-2\sqrt{15}})$$

$$sin6^{\circ}=cos84^{\circ}=\sin(36^{\circ}-30^{\circ})$$
$$=\frac{1}{8}(\sqrt{30-6\sqrt{5}}-\sqrt{5}-1)$$

$$sin9^{\circ}=cos81^{\circ}=\sin(45^{\circ}-36^{\circ})$$
$$=\frac{1}{8}(\sqrt{10}+\sqrt{2}-2\sqrt{5-\sqrt{5}})$$

$$sin12^{\circ}=cos78^{\circ}=\sin(30^{\circ}-18^{\circ})$$
$$=\frac{1}{8}(\sqrt{10+2\sqrt{5}}-\sqrt{15}+\sqrt{3})$$

$$sin21^{\circ}=cos69^{\circ}=\sin(36^{\circ}-15^{\circ})$$

$$=\frac{1}{8}(\sqrt{15-3\sqrt{5}}+\sqrt{5-\sqrt{5}}-\sqrt{10-5\sqrt{3}}$$
$$-\sqrt{2-\sqrt{3}})$$

$$sin24^{\circ}=cos66^{\circ}=\sin(54^{\circ}-30^{\circ})$$

$$=\frac{1}{8}(\sqrt{15}+\sqrt{3}-\sqrt{10-2\sqrt{5}})$$

$$sin27^{\circ}=cos63^{\circ}=\sin(45^{\circ}-18^{\circ})$$

$$=\frac{1}{8}(2\sqrt{5+\sqrt{5}}-\sqrt{10}+\sqrt{2})$$

$$sin33^{\circ}=cos57^{\circ}$$
$$=\sin(15^{\circ}+18^{\circ})$$
$$=\frac{1}{16}(2\sqrt{20+4\sqrt{5}-10\sqrt{3}-2\sqrt{15}}+\sqrt{30}+\sqrt{10}$$
$$-\sqrt{6}-\sqrt{2})$$

$$sin39^\circ = cos51^\circ = \sin(54^\circ - 15^\circ) = \frac{1}{16}(\sqrt{30} + \sqrt{6} + \sqrt{10} + \sqrt{2} - 2.\sqrt{20 + 2\sqrt{15} - 4\sqrt{5} - 10\sqrt{3}})$$

$$sin42^\circ = cos48^\circ = \sin(60^\circ - 18^\circ) = \frac{1}{8}(\sqrt{30 + 6\sqrt{5}} - \sqrt{5} + 1)$$

$$sin48^\circ = cos42^\circ = \sin(30^\circ + 18^\circ) = \frac{1}{8}(\sqrt{30 + 2\sqrt{5}} + \sqrt{15} - \sqrt{3})$$

$$sin51^\circ = cos39^\circ = \sin(36^\circ + 15^\circ) = \frac{1}{8}(\sqrt{15 - 3\sqrt{5}} - \sqrt{5 - \sqrt{5}} + \sqrt{10 - 5\sqrt{3}} + \sqrt{2 - \sqrt{3}})$$

$$sin57^\circ = cos33^\circ = \sin(72^\circ - 15^\circ) = \frac{1}{8}(\sqrt{15 + 3\sqrt{5}} - \sqrt{5 + \sqrt{5}} - \sqrt{10 - 5\sqrt{3}} + \sqrt{2 - \sqrt{3}})$$

$$sin63^\circ = cos27^\circ = \sin(45^\circ + 18^\circ) = \frac{1}{8}(2.\sqrt{5 + \sqrt{5}} + \sqrt{10} - \sqrt{2})$$

$$sin66^\circ = cos24^\circ = \sin(36^\circ + 30^\circ) = \frac{1}{8}(\sqrt{30 - 6\sqrt{5}} + \sqrt{5} + 1)$$

$$sin69^\circ = cos21^\circ = \sin(54^\circ + 15^\circ) = \frac{1}{16}(\sqrt{30} + \sqrt{10} + \sqrt{6} + \sqrt{2} + 2.\sqrt{20 + 2\sqrt{15} - 4\sqrt{5} - 10\sqrt{3}})$$

$$sin78^\circ = cos12^\circ = \sin(60^\circ + 18^\circ) = \frac{1}{8}(\sqrt{30 + 6\sqrt{5}} + \sqrt{5} - 1)$$

$$sin81^\circ = cos9^\circ = \sin(45^\circ + 36^\circ) = \frac{1}{8}(\sqrt{10} + \sqrt{2} + 2.\sqrt{5 - \sqrt{5}})$$

$$sin84^\circ = cos6^\circ = \sin(54^\circ + 30^\circ) = \frac{1}{8}(\sqrt{10 - 2\sqrt{5}} + \sqrt{15} + \sqrt{3})$$

$$sin87^\circ = cos3^\circ = \sin(72^\circ + 15^\circ) = \frac{1}{8}(\sqrt{15 + 3\sqrt{5}} + \sqrt{5 + \sqrt{5}} + \sqrt{10 - 5\sqrt{3}} - \sqrt{2 - \sqrt{3}})$$

As shown in the above equations, $3^\circ, 6^\circ, 9^\circ, 12^\circ, 15^\circ, 18^\circ, 21^\circ, 24^\circ, 27^\circ, 33^\circ, 39^\circ, 42^\circ, 48^\circ, 51^\circ, 57^\circ, 63^\circ, 66^\circ, 69^\circ, 78^\circ, 81^\circ, 84^\circ, 87^\circ$ sine and cosine trigonometric function values of angles, $\sqrt{2}, \sqrt{3}, \sqrt{5}, \sqrt{10}, \sqrt{15}, \sqrt{30}$ as they are calculated based on irrational numbers, their results are irrational (Beasley, 1858; Dörrie, 1950; Daut, 1951; Niven, 1956; Jung, 1962; Niven, 1964; Helton, 1972; Durell, 1975; Sigl, 1977; Barnet, 1991; Akarsu 2005; Akarsu, 2009; Bergen, 2009; Paolillo and Vincenzi, 2021). The rational and irrational values of trigonometric functions are used in applications of engineering sciences (Maune, 2001; Yakar, 2011; Pellicani et al. 2016; Alptekin et al. 2019; Ulvi et al., 2019; Alptekin, 2020).

4. Results and Discussion

Trigonometric functions are periodic functions with important applications in mathematics, science and technology. Trigonometric functions are widely used in science. Although rational numbers are numbers with finite decimal expansions, irrational numbers have infinite or noncyclic expansions. It has been shown by equations (13) that the trigonometric functions have infinitely many values in the 0^°≤α≤360^° definition range, while they have infinitely many irrational values in the -1≤sinα,cosα≤1 and-∞≤tanα≤∞ value ranges. As it can be understood from the examples given, it is understood from the examples (2.2.1), (2.2.2) and (2.2.3) above that although the rational values of the trigonometric functions in the value set are quite few, the majority of them consist of irrational numbers. Intermediate calculation values using trigonometric functions in basic sciences, astronomy, engineering and architecture, and technology contain rounding errors. Therefore, it is thought that it is important to be aware that the results of the calculations made with the irrational values of the trigonometric functions used in science always contain an error. It can be said that trigonometric functions, which are a simple geometric way of thinking, contribute to the development of today's science, mathematics, engineering and architectural education.

Author contributions

The article is single-authored.

Conflicts of interest

The authors declare no conflicts of interest.

Statement of Research and Publication Ethics

Research and publication ethics were complied with in the study.

References

Akarsu, V. (2005). Geometride, Uzay, Düşey ve Yatay Açılar Arasındaki Fonksiyonel İlişki, Selcuk Üniversity Journal of Engineering Sciences, 4(3), 134-142.

Akarsu, V. (2009). Düzlem Üçgende Açıların Kenarlardan Bulunması, Erciyes Üniversitesi Fen Bilimleri Enstitüsü Fen Bilimleri Dergisi, 25(1), 390-399.

Alptekin, A., & Yakar, M (2020). Heyelan bölgesinin İHA kullanarak modellenmesi. Türkiye İnsansız Hava Araçları Dergisi, 2(1), 17-21.

Alptekin, A., Çelik, M. Ö., Doğan, Y., & Yakar, M. (2019). Mapping of a rockfall site with an unmanned aerial vehicle. Mersin Photogrammetry Journal, 1(1), 12-16.

Barnet, R. A. (1991). Analytic Trigonometry with Applicattions, Wadsworth Publishing Company, Belmont, California, 431.

Beasley, R. D. (1858). Plane Trigonometry, Cambridge: Macmillan and Co., London, 106.

Bergen, J. (2009). Values of Trigonometric Functions, Math Horizons, 16(3), 17-19, DOI: 10.1080/10724117.2009.11974811

Britton, J. P., Proust, C., & Shnider, S. (2011). Plimpton 322: a review and a different perspective. Archive for history of exact sciences, 65, 519-566.

Daut, W. (1951). Ebene Trigonometrie, Paedagogischer Verlag Berthold Schulz, Berlin-Hannover-Frankfurt/Mein, 212.

Dörrie, H. (1950). Ebene und Sphaerische Trigonometrie, Verlag Von R. Oldenbourg, München, 518s.

Durell, C. V. (1975). Matriculation Trigonometry, G. Bell and Sons, Ltd, London, 151s.

Gölgeleyen F., & Akarsu V (2022). İnsan Aklının Evrimi: Lebombo Mağarası'ndan Mouseion'a Matematiğin Serüveni, Türkiye'de Mühendislik ve Mimarlığın 250 Yılı Uluslararası Sempozyumu, 19-21 Mayıs, İTÜ, İstanbul.

Helton, F. F. (1972). Analytic Trigonometry, W.B. Saunders Company, Philadelphia-London-Toronto, 297.

Jung, H. W. E. (1962). Sayılar Teorisine Giriş, Türk Matematik Derneği Yayınları, Çeviren: Orhan Ş. İçen, 176.

Mansfield, D. F., & Wildberger, N. J. (2017). Plimpton 322 is Babylonian exact sexagesimal trigonometry. Historia Mathematica, 44(4), 395-419.

Maune, D. F. (2001) Digital elevation model technologies and applications: The DEM User manual. The American Society for Photogrammetry and Remote Sensing. ISBN:1-57083-064-9

Niven, I. M. (1956). Irrational Numbers. Wiley, New York.

Niven, I. M. (1964). Rasyonel ve İrrasyonel Sayılar, Çeviri: Adnan Kıral, Türk matematik Derneği Yayınları, 192s.

Paolillo, B., & Vincenzi, G. (2021). On the rational values of trigonometric functions of angles that are rational in degrees. Mathematics Magazine, 94(2), 132-134.

Pellicani, R., Spilotro, G., & Van Westen, C. J. (2016). Rockfall trajectory modeling combined with heuristic analysis for assessing the rockfall hazard along the Maratea SS18 coastal road (Basilicata, Southern Italy). Landslides, 13, 985-1003.

Sigl, R. (1977). Ebene und Sphaerische Trigonometrie mit Anwendungen auf Kartographie, Geodaesie und Artonomie, Herbert Wichman Verlag, Karlsruhe, 50-55, 473.

Stewart I (2009). Timing The Infinite: The Story of Mathematics, Quercus, 336s.

Ulvi, A., Varol, F. i., Yiğit, A. Y. (2019). 3D modeling of cultural heritage: the example of Muyi Mubarek Mosque in Uzbekistan (Hz. Osman's Mushafi). International Congress on Cultural Heritage and Tourism (ICCHT), 115-123, Bishkek, Kyrgyzstan.

Van Brummelen, G. (2012). Heavenly mathematics: The forgotten art of spherical trigonometry. Princeton University Press.

Yakar, M (2011). Using close range photogrammetry to measure the position of inaccessible geological features. Experimental Techniques, 35(1), 54-59.

Advanced Geomatics

http://publish.mersin.edu.tr/index.php/geomatics/index

e-ISSN: 2791-8637

Forecasting of Water Levels by Artificial Neural Networks Technique in Lake Michigan-Huron

Mehmet Fehmi Yıldız [1], Vahdettin Demir*[1]

[1]KTO Karatay University, Faculty of Engineering and Natural Sciences, Civil Engineering Department, 42020, Konya, Türkiye; (mehmetfehmi.yildiz@ogrenci.karatay.edu.tr; vahdettin.demir@karatay.edu.tr)

Keywords

Lake Michigan-Huron,
ANN,
Lake water levels,
Forecasting.

Research Article

Received : 06.07.2023
Revised : 08.08.2023
Accepted : 12.09.2023
Published : 30.09.2023

* **Corresponding Author**
vahdettin.demir@karatay.edu.tr

Abstract

Water is an indispensable resource for all living things on Earth. Therefore, it is important to pay attention to current water consumption and to comply with safety precautions. Many water sources in the world experience ups and downs in the water level. Lake Michigan-Huron is an 8 km long body of water formed by the merging of Lake Michigan and Huron. The Huron and Michigan hydrological description is a single lake because the water from the Strait of Mackinac, which connects these lakes, balances what it expects. The flow is generally eastward, but the water moves in both directions depending on the local structure. Lake Michigan-Huron combined is the largest freshwater lake in the world. The aim of this study is to estimate the changes in water levels of Lake Michigan-Huron in the USA. In this study, the estimation of water levels on a monthly basis was investigated by using three different artificial neural network (ANN) models in order to predict the Michigan-Huron Lake water levels one month in advance. The ANN models used are Multilayer ANN (MANN), Radial Based ANN (RBANN) and Generalized Regression ANN (GRANN). The data sample consists of a 104-year (1918-2021) record of mean lake water level. 75% of all data were used for the training phase and 25% for the testing phase. Mean Absolute Error (MAE), Root Mean Square Error (RMSE) and coefficient of determination (R^2) were used as evaluation criteria. When the results are examined, all models give very good predictions during the training and testing phases. However, according to the test results, the model algorithms that give the most successful results are RBANN, MANN and GRANN, respectively.

1. Introduction

Humans have been interested in water since its inception, trying to study water movements, recognize features, identify detection hazards, and make the most of the water outside. The branch of science that manages the distribution and properties of water on Earth is called hydrology. The science of hydrology, which provides its relationship with the internal environment and efforts to control its environment, began to gain more importance. As a result of the hydrological operation, the basic structures that maintain their water consumption and attitudes can be identified (Koca, 2014).

Due to the changes in water bodies, long research has been started. Water is an indispensable resource for human life. Therefore, research on the quality and quantity of existing water resources has intensified, and the storage facility of closed water basins such as lakes has gained importance (Teltik et al., 2008).

The water level of many lakes in the world is observed to rise and fall due to various reasons. In the studies, it is thought that the reasons for the change in the lake level are meteorological and hydrological features (evaporation, precipitation, flow, etc.), tectonic movements, changes in the ozone layer and climate change (Teltik et al. 2008). In addition, the use of water resources to provide more water than normal in order to meet the water needs of agricultural activities and cities also causes the capacity of water reserves such as lakes to decrease (Albek et al., 2017). Some studies on the use of ANN in the literature, In the study of Desmukh and Tanty (2015), a comprehensive review was made on the artificial neural network (ANN) used in the field of hydrology-related problems. They stated that it can be

Cite this;

Yıldız, M. F. & Demir, V. (2023). Forecasting of Water Levels by Artificial Neural Networks Technique in Lake Michigan-Huron. Advanced Geomatics, 3(2), 63-71.

well exemplified by artificial intelligence with precipitation-flow modeling, stream flow modeling, water quality modeling and its applications in groundwater (Desmukh and Tanty 2015). In 2018, Arslan et al., A study was carried out to examine the seasonal variation of Adana Seyhan Dam Lake area. In their study, they achieved highly accurate results in the classification of water structures with the artificial neural network method (Arslan et al. 2018). A study was conducted by Aksoy et al. in 2020 on the estimation of the water level in Yalova Gökçe Dam using ANN. According to the data they obtained as a result of the analyzes, the dam water level for 2019 was 73.77, while the actual water level of the dam was measured as 72.13 meters. As a result, it is thought that the use of ANN algorithms will be beneficial in estimating the water level of Gökçe Dam (Aksoy et al. 2020). In 2012, Okkan and Dalkılıç conducted a study on the modeling of monthly flows of the Kemer Dam using radial-based neural networks. When they evaluated the results of their study in terms of minimum and maximum currents, the results of the RBANN model were successful for most months. In addition, it is thought that the problems encountered in other artificial neural network models can be overcome with RBANN (Okkan and Dalkılıç, 2012).

The purpose of this study was to analyze the water level of Lake Michigan-Huron in the United States and to determine changes in the lake's water level. For this purpose, monthly lake water levels in Lake Michigan-Huron between 1918-2021 were estimated with radial-based artificial neural networks and the predictions in various data sets (the training set is 3 parts, and the test set is 1 part, and the test set is constantly changing.) were compared with the observed data.

2. Material And Method

2.1. Material

In the study, monthly water levels year from January 1918 to December 2021 were used. Data obtained from "https://www.lre.usace.army.mil/Missions/Great-Lakes-Information/Great-Lakes-Information.aspx#ICG_ETH_22302". Statistical information of the data used is given in Table 1.

The data are monitored as monthly average (m) and there are no discontinuities in the data. In addition, station information in Excel format is available for all researchers free of charge.

Table 1. Statistical information for water levels (m)

Michigan-Huron	
Average	176.44
Standard error	0.0116
Median	176.45
Standard Deviation	0.410
Sample Variance	0.168
Kurtosis	-0.787
Skewness	0.101
Smallest	175.57
Largest	177.5
Number of Data	1248

75% of all data were used in the training phase and 25% in the testing phase. At this stage, four different combinations of training (75%) and testing (25%) were tried (Figure 1).

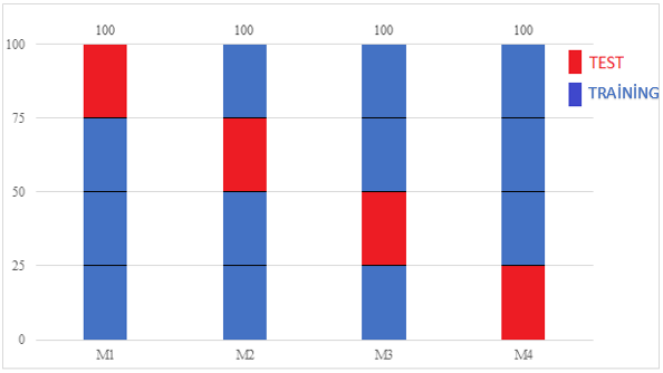

Figure 1. Percentage of training and testing data

Correlation analysis was performed using the MATLAB program to better understand the input combinations in the models and is visualized in Figure 2.

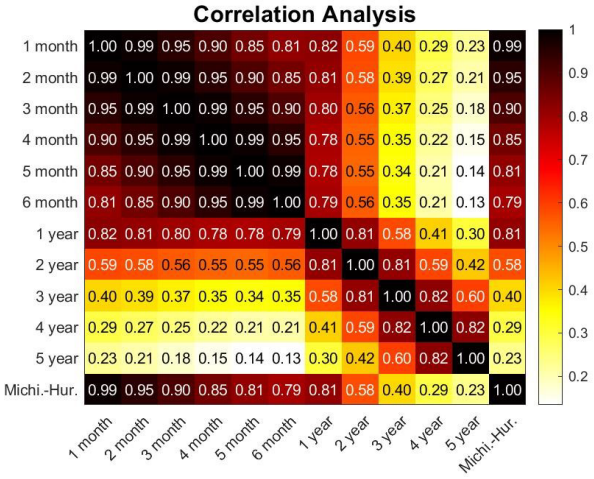

Figure 2. Correlation matrix

Figure 2 shows the correlation values of the input data. Looking at the table, it is seen that the correlation coefficient decreased and the relationship between the variables decreased after the 2nd year.

2.2. Study Area

Lake Michigan is the third largest of the five great lakes in the northern United States and is connected to Lake Huron by the Strait of Mackinac (Demir, 2022). It is located 176 meters above sea level and its deepest point is 281 meters. Lake Huron is also located in North America and is the 4th largest lake in the world.

Lake Huron is connected to Lake Michigan by the Straits of Mackinac and to Lake Superior by a series of straits. Huron and Michigan are hydrologically a single lake because the flow of water through the straits keeps water levels in overall balance. Although the flow is generally eastward, water moves in both directions depending on local conditions. Combined, Lake Michigan-Huron is the world's largest freshwater lake by area (Michigan-Huron, 2023). The study area is given in Figure 3.

Figure 3. Lake Michigan-Huron (Demir and Yaseen, 2022)

The most important factor in choosing this study area is that when Michigan-Huron Lake is considered as a whole, it is the largest freshwater lake in the world in terms of surface area and the data are continuous.

2.3. Method

ANN are a method based on the biological nervous system in humans. ANN consist of elements called neurons, which are connected in parallel and have a non-linear structure. It is used in object recognition, system modeling, signal processing and solving complex engineering problems. Artificial neural networks realize the learning process with examples. In other words, it can be defined as the machine-transferred version of the human learning mechanism (D'Addona, 2014).

In this study, 3 different ANN models were used, namely Radial Based Artificial Neural Networks, Generalized Regression Artificial Neural Networks and Multilayer Artificial Neural Networks.

2.4. Radial Based Neural Network

RBANN model can be considered as a combination of a data modeling technique for a high-dimensional space and a schema such as an ANN network. In the RBANN model, three layers are defined as input layer, hidden layer and output layer, but unlike the classical ANN structure, a nonlinear clustering analysis and radial based activation functions are used in the transition from the input layer to the hidden layer in the radial-based neural network model
(Okkan and Dalkılıç, 2012).

The mathematical representation of radial basis neural networks is as follows.

$$\emptyset_j = exp\lfloor -\|x - c_j\|/\sigma_j^2 \rfloor \quad (1)$$

Here is x the input vector, $c_{\bar{j}}$ j. It is the center of the Gaussian function and $\sigma_{\bar{j}}$ is the standard deviation. Equation $\|x - c_{\bar{j}}\|$ indicates the Euclidean distance between vectors x and $c_{\bar{j}}$. j. the activation level of the intermediate node is equal to $\emptyset_{\bar{j}}$ .Interlayer outputs;

$$y_{ki} = \pi\emptyset_i(x, c, \sigma) \quad (2)$$

k. the output of the node is given by Equation 2.

$$o_k = \sum_{j=1}^{J} w_{kj} y_{kj} \quad (3)$$

Here $w_{k\bar{j}}$ k. With the exit node $\bar{j}$. is the weight between the middleware node (Kılıç et al., 2012). The basic structure of RBANN is given in Figure 4.

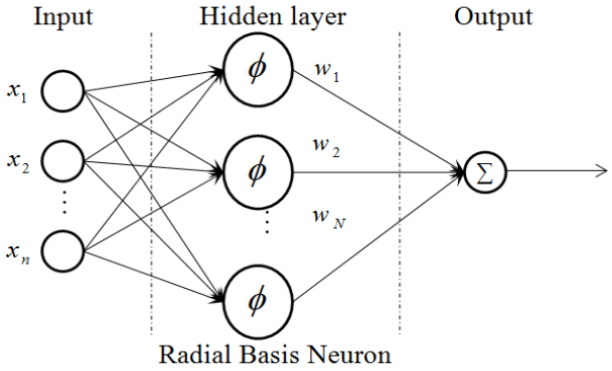

Figure 4. Radial-based neural network structure (Chen et al. 2019)

In Figure 4, the RBANN structure basically consists of three parts and the output data is obtained by multiplying the input data with the weights after reaching the hidden layer.

2.5. Generalized Regression Artificial Neural Network

GRANN does not require an iterative training procedure like the back propagation method. In this model, an approximate estimation function is generated directly from the training data. In addition, in the GRANN model, when the size of the training data is large, the estimated error approaches zero with a slight restriction in the function. By definition, regression predicts the most likely value of a dependent variable "y" based on the independent variable "x" given "x" and the training set. GRANN is a method that estimates the joint Probability Density Function of "x" and "y" given a training set. Since the probability density function is obtained from the data without pre-acceptance, the system is generally ideal. The basic structure of GRANN is given in Figure 5.

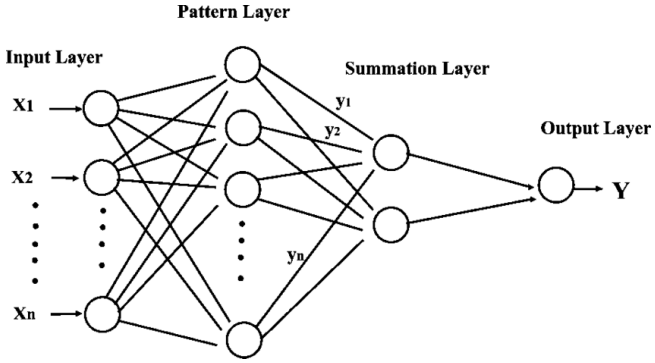

Figure 5. Generalized regression artificial neural network structure (Usluoglu et al. 2008)

2.6. Multilayer Neural Network

MANN is one of the most widely used artificial neural network models. In multilayer artificial neural networks, neurons are organized in layers. The first layer is the input layer, and it provides the information about the problem to be solved to the ANN. Another layer is the output layer, where the processed information is transmitted to the outside. There is a hidden layer between the input and output layers. Multilayer neural networks can have more than one hidden layer. In the MANN model, it is feed-forward because forward information flow occurs. It propagates backwards until the error is minimal. The basic structure of MANN is given in Figure 6.

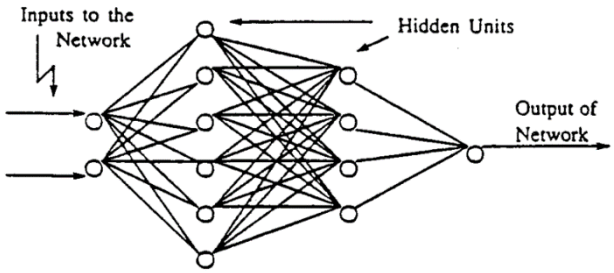

Figure 6. Multilayer neural network structure (Ciliz and Isik, 1996)

3. Results

In the modeling phase, the data were first shifted by lag time, and then the estimation results were obtained by separating them into training and test sets. The estimated data with the observed data were evaluated by considering the comparison criteria. Root Mean Square Error (RMSE), Mean Absolute Error (MAE) and coefficient of determination (R^2) were used as comparison criteria. The formulas of the comparison criteria are given in Equation 4-6.

$$RMSE = \sqrt{\frac{1}{N}\sum_{i=1}^{N}(Y_p - Y_o)^2} \quad (4)$$

$$MAE = \frac{1}{N}\sum_{i=1}^{N}|Y_p - Y_o| \quad (5)$$

$$R^2 = \left(\frac{N*(\sum Y_o*Y_p)-(\sum Y_o)*(\sum Y_p)}{\sqrt{(N*\sum Y_o^2)-(\sum Y_o)^2*(N*\sum Y_p^2)-(\sum Y_p)^2}}\right)^2 \quad (6)$$

N is the number of data used in the equations, Yp represents the estimated value in the model, Yo represents the observed value. Since Equation (4-5) has error results for our comparison criteria, the unit of error results in the model is m.

High error results show that the model is far from real data, that is, it gives unsuccessful results. If the error values are close to zero, it indicates that the results of the model are close to the real data.

The coefficient of determination R^2 can take a value between 0 and 1. It is interpreted that the closer the value is to 1, the higher the model's fitness and accuracy.

In the study, data sets with 12 inputs were created (Figure 2). These; 1 month lag (T-1), T-2, T-3, T-4, T-5 and T-6 with 1 year lag (Y-1), Y-2, Y-3, Y-4 and Y-5.

Month numbers representing the periodicity of the data were used recursively as the 12th input set. 75% of all data were used in the training phase and 25% in the testing phase. At this stage, four different combinations were tried, namely training (75%) and testing (25%). These are M1 (the part with the oldest data), M2, M3 and M4 (the part with the most recent data). Model results are given in Tables 2-3-4 according to the training and testing phases. The flow chart of the study is given in Figure 7.

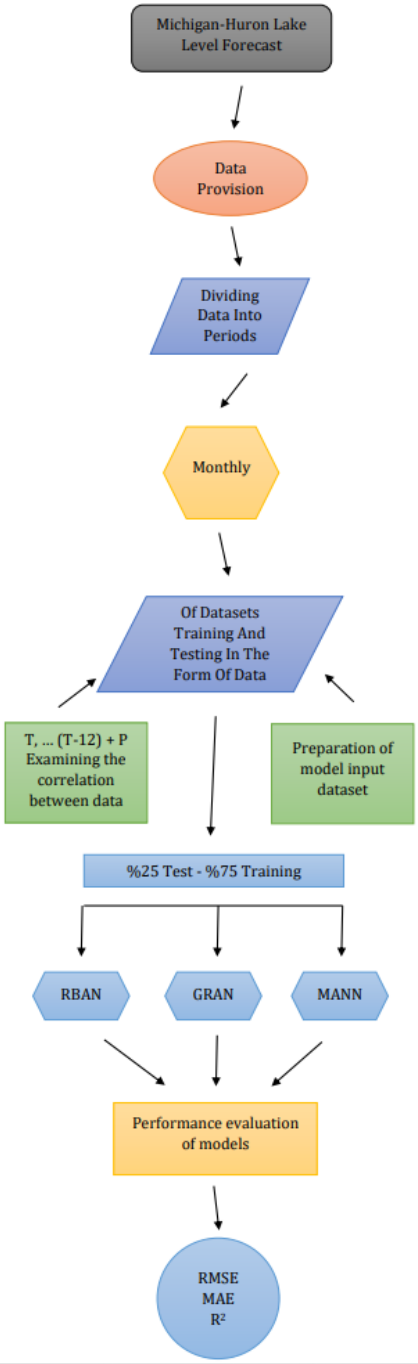

Figure 7. Flow chart of study

Table 2. RBANN training and test results

		Inputs	Training			Testing		
			RMSE	MAE	R^2	RMSE	MAE	R^2
RBANN	M1	1	0.069	0.055	0.970	0.066	0.054	0.964
		2	0.046	0.037	0.986	0.044	0.035	0.984
		3	0.044	0.034	0.987	0.042	0.033	0.986
		4	0.043	0.033	0.988	0.041	0.031	0.987
		5	0.042	0.033	0.989	0.039	0.030	0.987
		6	0.042	0.032	0.989	0.039	0.030	0.988
		7	0.041	0.032	0.989	0.038	0.030	0.988
		8	0.041	0.032	0.989	0.038	0.030	0.988
		9	0.042	0.032	0.989	0.039	0.031	0.987
		10	0.042	0.033	0.988	0.040	0.031	0.987
		11	0.043	0.033	0.988	0.040	0.031	0.987
		12	0.039	0.030	0.990	0.038	0.030	0.988
	M2	1	0.067	0.054	0.973	0.071	0.057	0.962
		2	0.045	0.036	0.988	0.048	0.037	0.983
		3	0.043	0.034	0.989	0.045	0.035	0.985
		4	0.042	0.033	0.989	0.044	0.034	0.986
		5	0.042	0.033	0.989	0.043	0.033	0.986
		6	0.041	0.031	0.990	0.042	0.032	0.987
		7	0.041	0.032	0.990	0.041	0.031	0.988
		8	0.040	0.032	0.990	0.041	0.031	0.988
		9	0.041	0.032	0.990	0.042	0.031	0.987
		10	0.042	0.033	0.989	0.043	0.032	0.987
		11	0.042	0.033	0.989	0.042	0.032	0.987
		12	0.039	0.031	0.991	0.040	0.031	0.988
	M3	1	0.069	0.055	0.964	0.066	0.054	0.945
		2	0.045	0.036	0.985	0.049	0.039	0.973
		3	0.043	0.034	0.986	0.046	0.036	0.975
		4	0.042	0.032	0.987	0.045	0.035	0.976
		5	0.041	0.032	0.987	0.044	0.034	0.977
		6	0.040	0.031	0.988	0.042	0.033	0.978
		7	0.040	0.031	0.988	0.043	0.033	0.978
		8	0.040	0.031	0.988	0.044	0.034	0.977
		9	0.040	0.031	0.988	0.044	0.035	0.977
		10	0.041	0.032	0.987	0.044	0.035	0.976
		11	0.042	0.032	0.987	0.047	0.037	0.975
		12	0.040	0.031	0.988	0.046	0.036	0.976
	M4	1	0.068	0.055	0.971	0.068	0.055	0.963
		2	0.048	0.038	0.985	0.046	0.037	0.983
		3	0.044	0.034	0.988	0.044	0.035	0.984
		4	0.042	0.033	0.989	0.042	0.033	0.986
		5	0.041	0.032	0.989	0.041	0.033	0.986
		6	0.040	0.031	0.990	0.042	0.033	0.986
		7	0.040	0.031	0.990	0.041	0.032	0.987
		8	0.040	0.031	0.990	0.042	0.033	0.986
		9	0.041	0.032	0.990	0.042	0.033	0.986
		10	0.041	0.032	0.989	0.042	0.033	0.986
		11	0.042	0.032	0.989	0.043	0.034	0.985
		12	0.039	0.030	0.990	0.040	0.032	0.987

In the Table 2, the most successful result in the test phase was obtained in 7 inputs. The scatter plot of the best method is given in Figure 8.

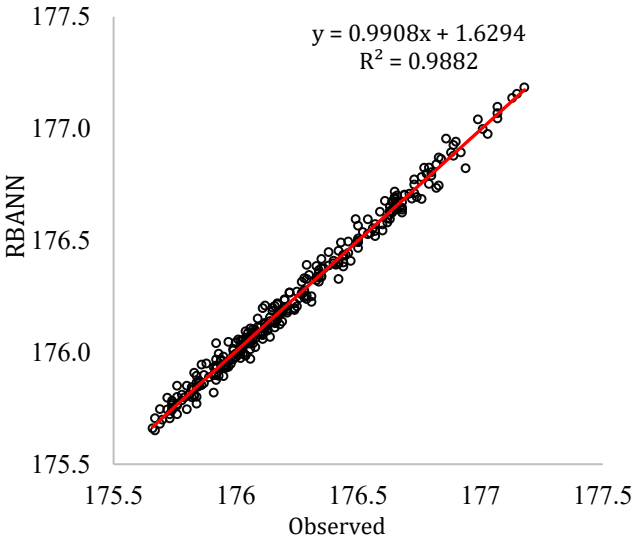

Figure 8. Scatter plot

When the values in the graph are examined, it is seen that the results obtained using the radial-based artificial neural network model are compatible with the water level data of the observed lake, and the graph equation approaches the y=x line, and the R^2 value is 0.9882. The variation of these estimates in the time series is shown in Figure 9.

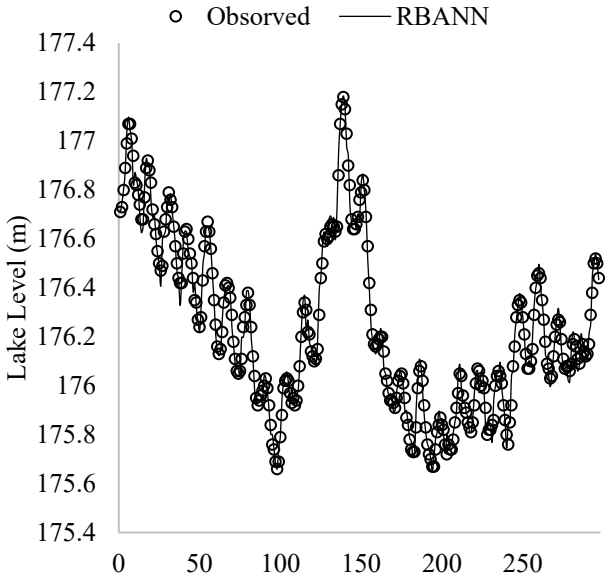

Figure 9. Timeline graph of test data

Figure 9 shows the estimates of test data for the M1 package. RBANN appears to capture the highs and lows of the test data well. It is clearly seen that the model is able to capture the highest and lowest data.

Table 3. GRANN training and test results

		Inputs	Training			Testing		
			RMSE	MAE	R^2	RMSE	MAE	R^2
GRANN	M1	1	0.066	0.053	0.972	0.069	0.055	0.962
		2	0.024	0.017	0.996	0.060	0.049	0.971
		3	0.010	0.004	0.999	0.065	0.051	0.966
		4	0.004	0.001	1.000	0.071	0.057	0.960
		5	0.002	0.000	1.000	0.078	0.062	0.952
		6	0.001	0.000	1.000	0.085	0.066	0.943
		7	0.001	0.000	1.000	0.100	0.081	0.920
		8	0.000	0.000	1.000	0.118	0.095	0.891
		9	0.000	0.000	1.000	0.139	0.112	0.853
		10	0.000	0.000	1.000	0.157	0.126	0.815
		11	0.001	0.000	1.000	0.175	0.139	0.778
		12	0.000	0.000	1.000	0.134	0.108	0.860
	M2	1	0.065	0.053	0.974	0.072	0.058	0.962
		2	0.025	0.018	0.996	0.062	0.049	0.971
		3	0.012	0.007	0.999	0.071	0.056	0.963
		4	0.005	0.002	1.000	0.073	0.058	0.962
		5	0.002	0.001	1.000	0.076	0.061	0.957
		6	0.001	0.000	1.000	0.082	0.064	0.951
		7	0.001	0.000	1.000	0.102	0.081	0.929
		8	0.002	0.001	1.000	0.134	0.110	0.867
		9	0.002	0.001	1.000	0.150	0.120	0.836
		10	0.003	0.001	1.000	0.168	0.138	0.800
		11	0.003	0.001	1.000	0.172	0.140	0.791
		12	0.000	0.000	1.000	0.149	0.121	0.843
	M3	1	0.066	0.053	0.967	0.073	0.059	0.934
		2	0.027	0.019	0.994	0.065	0.050	0.949
		3	0.017	0.010	0.998	0.077	0.060	0.928
		4	0.010	0.005	0.999	0.084	0.065	0.916
		5	0.006	0.002	1.000	0.092	0.070	0.902
		6	0.006	0.002	1.000	0.101	0.076	0.884
		7	0.001	0.000	1.000	0.117	0.088	0.835
		8	0.002	0.000	1.000	0.146	0.113	0.757
		9	0.001	0.000	1.000	0.142	0.113	0.788
		10	0.001	0.000	1.000	0.156	0.122	0.761
		11	0.002	0.000	1.000	0.181	0.144	0.727
		12	0.000	0.000	1.000	0.155	0.123	0.791
	M4	1	0.066	0.053	0.973	0.070	0.056	0.961
		2	0.026	0.018	0.996	0.059	0.047	0.972
		3	0.010	0.005	0.999	0.065	0.052	0.967
		4	0.004	0.001	1.000	0.068	0.054	0.964
		5	0.002	0.000	1.000	0.074	0.057	0.956
		6	0.001	0.000	1.000	0.083	0.064	0.945
		7	0.000	0.000	1.000	0.095	0.075	0.929
		8	0.001	0.000	1.000	0.122	0.094	0.884
		9	0.001	0.000	1.000	0.139	0.110	0.855
		10	0.001	0.000	1.000	0.154	0.122	0.824
		11	0.001	0.000	1.000	0.160	0.127	0.804
		12	0.000	0.000	1.000	0.139	0.113	0.849

In the Table 3, the most successful result in the test phase was obtained in 2 inputs. The scatter plot of the best method is given in Figure 10.

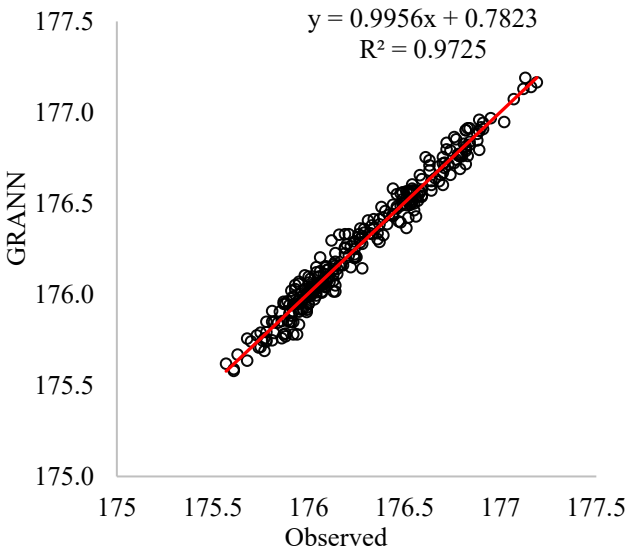

Figure 10. Scatter plot

When the values in the graph are examined, it is seen that the results obtained using the GRANN model are compatible with the water level data of the observed lake, and the graph equation approaches the y=x line, and the R^2 value is 0.9725. As the coefficient of determination approaches 1 in the scatterplot, the model and the estimations overlap. In other words, the model can give more accurate predictions. The variation of these estimates in the time series is shown in Figure 11.

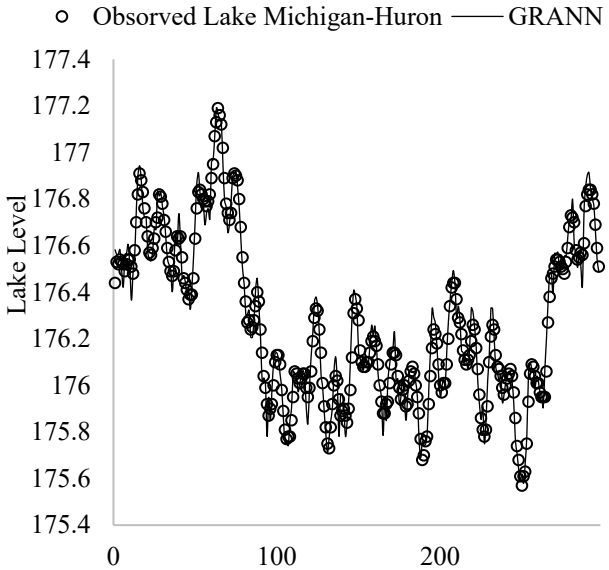

Figure 11. Timeline graph of test data

Figure 11 shows estimates of test data for the M4 package. GRANN seems to capture almost all the data. Although the lake water level fluctuations show instantaneous changes in the time series, it is seen that the model catches these changes.

Table 4. MANN training and test results

		Inputs	Training			Testing		
			RMSE	MAE	R^2	RMSE	MAE	R^2
MANN	M1	1	0.069	0.055	0.970	0.067	0.054	0.964
		2	0.047	0.037	0.986	0.045	0.035	0.984
		3	0.043	0.034	0.988	0.044	0.034	0.984
		4	0.045	0.035	0.987	0.042	0.033	0.985
		5	0.042	0.032	0.989	0.040	0.031	0.987
		6	0.039	0.030	0.990	0.039	0.030	0.987
		7	0.039	0.030	0.990	0.039	0.030	0.988
		8	0.039	0.030	0.990	0.038	0.030	0.988
		9	0.038	0.030	0.991	0.040	0.031	0.987
		10	0.040	0.031	0.990	0.039	0.031	0.987
		11	0.039	0.030	0.990	0.048	0.035	0.981
		12	0.042	0.033	0.989	0.040	0.030	0.987
	M2	1	0.067	0.054	0.973	0.072	0.058	0.962
		2	0.208	0.166	0.736	0.254	0.210	0.529
		3	0.045	0.035	0.988	0.046	0.035	0.985
		4	0.042	0.032	0.989	0.045	0.034	0.985
		5	0.041	0.032	0.990	0.044	0.034	0.986
		6	0.041	0.032	0.990	0.043	0.033	0.987
		7	0.039	0.030	0.991	0.041	0.031	0.988
		8	0.039	0.030	0.991	0.041	0.031	0.988
		9	0.040	0.031	0.990	0.043	0.033	0.986
		10	0.042	0.033	0.989	0.042	0.032	0.987
		11	0.038	0.030	0.991	0.044	0.034	0.986
		12	0.043	0.033	0.989	0.044	0.033	0.986
	M3	1	0.069	0.055	0.964	0.068	0.055	0.943
		2	0.045	0.036	0.984	0.049	0.039	0.973
		3	0.044	0.034	0.985	0.050	0.038	0.973
		4	0.042	0.032	0.987	0.046	0.036	0.975
		5	0.041	0.031	0.987	0.045	0.035	0.976
		6	0.041	0.032	0.987	0.049	0.038	0.973
		7	0.038	0.029	0.989	0.045	0.034	0.977
		8	0.039	0.030	0.989	0.044	0.034	0.978
		9	0.040	0.031	0.988	0.045	0.035	0.976
		10	0.038	0.029	0.989	0.051	0.038	0.971
		11	0.038	0.029	0.989	0.055	0.042	0.968
		12	0.034	0.026	0.991	0.039	0.031	0.982
	M4	1	0.068	0.055	0.971	0.069	0.055	0.962
		2	0.047	0.038	0.986	0.046	0.036	0.983
		3	0.044	0.034	0.988	0.045	0.036	0.984
		4	0.044	0.034	0.988	0.045	0.035	0.984
		5	0.041	0.031	0.990	0.042	0.033	0.986
		6	0.041	0.031	0.990	0.042	0.034	0.986
		7	0.038	0.029	0.991	0.042	0.033	0.986
		8	0.038	0.029	0.991	0.042	0.033	0.986
		9	0.037	0.029	0.991	0.047	0.035	0.983
		10	0.038	0.029	0.991	0.043	0.035	0.985
		11	0.038	0.030	0.991	0.043	0.034	0.985
		12	0.043	0.033	0.988	0.043	0.034	0.985

In the Table 4, the most successful result in the test phase was obtained in 8 inputs. The scatter plot of the best method is given in Figure 12.

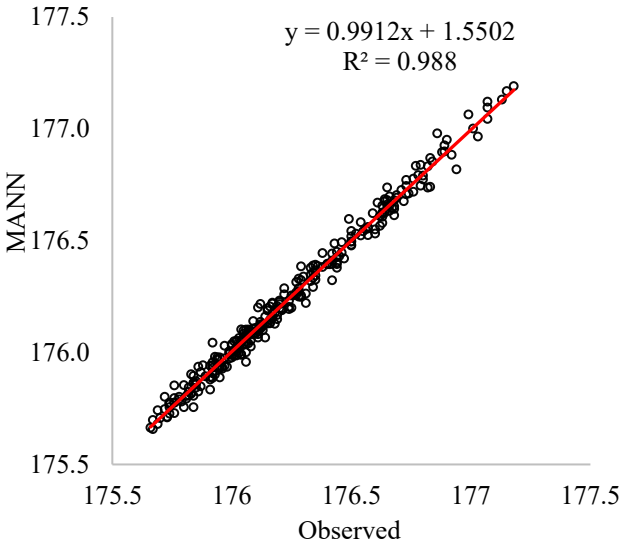

Figure 12. Scatter plot

When the values in the graph are examined, it is seen that the results obtained using the MANN model are compatible with the water level data of the observed lake, and the graph equation approaches the y=x line, and the R^2 value is 0.988. The variation of these estimates in the time series is shown in Figure 13.

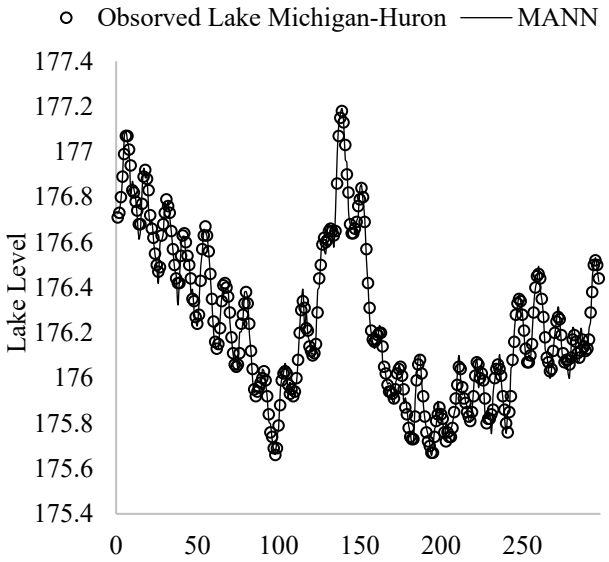

Figure 13. Timeline graph of test data

Figure 13 shows the estimates of test data for the M1 package. MANN appears to capture the highs and lows of the test data well.

4. Discussion

In a study conducted by Çubukçu et al. in 2021 on the estimation of the monthly average water levels of Lake Michigan, data between 1981 and 2021 were used and studied with three different artificial neural network models. These models are multilayer ANN, radial basis

ANN and generalized ANN models. RMSE, MAE and R^2 were used as comparison criteria. In general, it was seen that all models gave good results, but according to the test results, the best training algorithm was seen as multilayer ANN, giving the best results in 12 inputs. (MAE= 0.0342, RMSE= 0.0435, R^2= 0.9906). The best method was found to be MANN, RBANN and GRNN, respectively (Çubukçu et al. 2021).

Çalım conducted a study in 2008 on the estimation of dam reservoir elevation using artificial neural networks. ANN models were used in the study. When the results obtained using ANN are compared with the results obtained with different methods before, it is concluded that ANN models perform better than the classical methods used in the past (Çalım, 2008).

In a study conducted by Dikbaş and Fırat in 2005, a comparison of POM and ANN models was made in three-dimensional hydrodynamic modeling in lakes. When the results obtained with both models were compared, it was seen that the methods had advantages and disadvantages compared to each other. ANN requires previously obtained observation results and calculations, while POM does not. In addition, ANN achieves results in a much shorter time than POM. As a result, it can be recommended to use the artificial neural network method in certain sections and studies that require many detailed calculations (Dikbaş and Fırat, 2005).

In a study conducted by Demir in 2021, the water level changes of Lake Michigan were examined using MARS, M5-tree and LSSVR methods. These three models have gone through training and testing phases. RMSE, MAE and R^2 were used as evaluation criteria. In the study, 80% of the data was used in the training phase and the remaining 20% in the testing phase. The data period of the study is between 1918 and 2020. Data deferred up to 8 months were used as the input set. When the results were examined, it was seen that better results were obtained with the MARS method (RMSE=0.0359, MAE=0.0288, R^2=0.9922). In addition, it was stated that the periodicity effect increased the model performance. (Demir, 2022).

In a study conducted by Özaydın in 2009, the estimation of the water reservoir level of Eskişehir badger dam was studied. In this study, artificial neural networks and ARMAX model were used as methods and these two models were compared with each other. Data from January 1973 to December 2006 were used. As a result of the analyzes made, it has been seen that the results obtained with artificial neural networks are closer to the truth than the results obtained with the ARMAX method (Özaydın, 2009).

In 2009, a study was conducted by Yarar and Onuçyıldız on the determination of water level changes in Beyşehir Lake with artificial neural networks. In this study, data belonging to the years 1962-1990 were used. The data between 1962-1985 was used for training, and the data between 1985-1990 was used for testing. As a method, back propagation multilayer ANN model was chosen due to its widespread use and 3 different algorithms, Levenberg-Marquardt, One-Step Secant and Scaled Matched Gradient, were used. The smallest error 0.056285 was obtained for the 1 hidden layer, 7 hidden nodes and 500 epochs in the Scaled Matching Gradient model from these three different models. The data obtained by ANN models were compared with the data obtained by classical methods, and it was concluded that the use of ANN models would be beneficial in estimating the water level of Beyşehir Lake (Yarar and Onuçyıldız, 2009).

In 2010, a study was conducted on the use of artificial neural networks in river flow prediction. The Blue Nile River in Sudan was chosen as the study area. Four different ANN models were used in the study. The common feature of the four selected models was that they had a multi-layer perceptron structure. All four models use the precipitation index as a common input. ANN1 only uses this common input, while ANN2 and ANN3 use seasonal precipitation expectation or seasonal flow expectation as additional input. ANN4 uses both the seasonal flow forecast and the seasonal precipitation forecast. When the results are examined, it is seen that the ANN4 model gives the most successful result (highest R^2). The results of the study show that the selection of appropriate inputs in the ANN model directly affects the success of the model (Shamseldin, 2010).

The methods used in this study and the findings obtained are compatible and supportive with the performances obtained in previous studies in the literature.

5. Conclusion

In this study, using the monthly average lake water level data of Lake Michigan-Huron between 1918 and 2021, predictions were made with different ANN methods and the results were compared. In the study, 75% of all data were used in the training phase and 25% in the testing phase. At this stage, four different combinations of training (75%) and testing (25%) were tried. Mean Absolute Error (MAE), Root Mean Square Error (RMSE), coefficient of determination (R^2) were used as evaluation criteria. The results are as follows:

- When the Tables 2-4 obtained with 3 different models are examined, it is seen that all models do very well in the training and testing stages, seem to make predictions.
- When the training results are compared, after GRANN (RMSE=0.000012, R^2=0.9998), which has the least error with the evaluation criteria, are MANN (RMSE=0.0337, R^2=0.9914) and RBANN (RMSE =0.0386, R^2=0.9910), respectively.
- According to the test results, the model algorithm that gives the most successful result is RBANN (RMSE=0.0381, R^2=0.9881). Best result in 7 entries seems to give. The best method for the testing phase is RBANN, MANN, and GRANN, respectively.

As a result, it is thought that the use of ANN algorithms will be useful in estimating the Michigan-Huron lakes water level.

Acknowledgement

This is the extended version of the paper titled "Lake Level Estimation with Radial Based Artificial Neural Networks" presented at the 6th IGD Symposium of Mersin University.

The authors thank the U.S. Army Corps of Engineers for providing Michigan-Huron Territory data. The authors also thank KTO Karatay University and Mersin University.

Author contributions

Mehmet Fehmi Yıldız: Data supply, Writing-Original Draft Preparation, Revision.
Vahdettin Demir: Investigation, Methodology, Software, Revision.

Conflicts of interest

There is no conflict of interest between the authors.

Statement of Research and Publication Ethics

Research and publication ethics were complied with in the study.

References

Aksoy, A. S., Aksoy, Y. R., Keskin, M. E., & Yılmazkoç, B., (2017). Göl Seviye Tahmini: Eğirdir Gölü: Mühendislik Bilimleri ve Tasarım Dergisi., 5(3), 601-608.

Albek, E. A., Albek, M. & Göncü, S. (2017). Trend Analysis of Burdur, Eğirdir, Sapanca and Tuz Lake Water Levels Using Nonparametric Statistical Methods. Afyon Kocatepe University Journal of Sciences and Engineering, 17(2), 555–570.

Arslan, N., Çiçekli, S., Dönmez, C., Şekertekin, A., (2018). Adana Seyhan Baraj Gölü Alanının Mevsimsel Değişiminin Yapay Sinir Ağları ile Analizi. Uzaktan Algılama ve Coğrafi Bilgi Sistemi Sempozumu, Ankara.

Chen, T., Cheng, P., He, H., Yan, Y., (2019). Tree Height Estimation of Forest Plantation in Mountainous Terrain from Bare-Earth Points Using a DoG-Coupled Radial Basis Function Neural Network., 11,1271.

Ciliz, M. K., & Işik, C., (1997). On-Line Learning Control of Manipulators Based On Artificial Neural Network Models. Robotica, 15(3), 293–304. doi:10.1017/s0263574797000337

Çalım, M.M., (2008). Yapay Sinir Ağları Yöntemi ile Baraj Hazne Kotu Tahmini., Yüksek Lisans Tezi, Mustafa Kemal Üniversitesi, Fen Bilimleri Enstitüsü, Hatay,61p.

Çubukçu, E. A., Yılmaz C. B., Demir, V., & Sevimli, M. F. (2021). Forecasting Of Monthly Average Lake Levels Of Lake Michigan With Artificial Neural Networks. 1st Advanced Engineering Days, 4-7.

D'Addona D.M. (2014). Neural Network, in: CIRP Encycl. Prod. Eng., Springer Berlin Heidelberg, Berlin, Heidelberg, 2014: pp. 911–918. https://doi.org/10.1007/978-3-642-20617-7_6563.

Demir, V. (2022) Enhancing Monthly Lake Levels Forecasting Using Heuristic Regression Techniques with Periodicity Data Component: Application Of Lake Michigan. Theor Appl Climatol 148, 915–929. https://doi.org/10.1007/s00704-022-03982-0

Demir, V., Yaseen, Z. M., (2022). Neurocomputing Intelligence Models for Lakes Water Level Forecasting: A Comprehensive Review. Neural Computing and Applications 2023 (35), 303–343

Desmukh, T., Tanty, R., (2015). Application of Artificial Neural Network in Hydrology- A Review. International Journal of Engineering Research and Technology, 4(6), 184-188.

Dikbaş, F., Fırat, M., (2006). Göllerde Üç Boyutlu Hidrodinamik Modellemede POM ve Yapay Sinir Ağları Yöntemlerinin Kullanılması: Gökpınar Baraj Gölü Örneği: Mühendislik Bilimleri Dergisi., 1(12), 43-50.

Kılıç, E., Özbalcı, Ü., & Özçalık, H. R. (2012). Comparison of MLP and RBF Structures in Modeling of Nonlinear Dynamic Systems with Artificial Neural Networks, Elektrik - Elektronik ve Bilgisayar Mühendisliği Sempozyumu, 29 Kasım - 01 Aralık 2012, Bursa.

Koca, Y. (2014). Rize İyidere Alt Havzası İkİzdere Kesiti İçin Birim Hidrografın Belirlenmesi. Uzmanlık tezi, Orman ve Su İşleri Bakanlığı, Ankara, 68p.

Michigan-Huron (2023), Lake Michigan–Huron https://en.wikipedia.org/wiki/Lake_Michigan%E2%80%93Huron, Access date: 25.05.2023

Okkan, U. & Dalkılıç, H. (2012). Radyal Tabanlı Yapay Sinir Ağları ile Kemer Barajı Aylık Akımlarının Modellenmesi. Teknik Dergi , 23 (112) , 5957-5966.

Özaydın, Ö., (2009). ARMAX Modelleri ve Porsuk Barajı Su Seviyesinin Öngörüsü. Doktora Tezi, Eskişehir Osmangazi Üniversitesi, Fen Bilimleri Enstitüsü, İstatistik Anabilim Dalı, Eskişehir.

Shamseldin A. Y., (2010), ANN Model for River Flow Forecasting in A Developing Country, Journal of Hydroin formatics, 12 (1), 22–35.

Teltik İ., Aksoy H., Ünal N.E., (2008). Van Gölü Su Seviyesi Stokastik Modelleri, Van Gölü Hidrolojisi ve Kirliliği Konferansı, 21-22 Ağustos 2008, DSİ XVII. Bölge Müdürlüğü, Van, s. 74-81.

Ustaoglu B., Cigizoglu H. K., Karaca M., (2008) Forecast of Daily Mean, Maximum and Minimum Temperature Time Series by Three Artificial Neural Network Methods, Meteorological Applications 15, 431–445.

Yarar, A., Onüçyıldız, M., (2009). Yapay Sinir Ağlari ile Beyşehir Gölü Su Seviyesi Değişimlerinin Belirlenmesi., Selçuk Üniversitesi Mühendislik Mimarlık Fakültesi Dergisi, 24(2), 21-30.

Advanced Geomatics

http://publish.mersin.edu.tr/index.php/geomatics/index

e-ISSN: 2791-8637

Temporal Change of Göksu River

Hakan Satılmış[1], Özşen Çorumluoğlu[1], Elif Akyel[*1]

[1]İzmir Katip Çelebi University, Geomatics Engineering, 35620, İzmir, Türkiye; (hakansatilmis_@outlook.com; ozsen.corumluoglu@ikcu.edu.tr; elif.akyel@ikcu.edu.tr)

Keywords

River Course,
Vegetation Region,
Unsupervised Classification,
NDWI,
NDVI.

Research Article

Received : 22.02.2023
Revised : 08.08.2023
Accepted : 11.09.2023
Published : 30.09.2023

* **Corresponding Author**
elif.akyel@ikcu.edu.tr

Abstract

Rivers meet the agricultural and energy needs of people and living things. In addition, it is the most important external factor and process in the shaping of the surface where we live. Turkey is a very rich country in terms of rivers and wetlands in general. Göksu River, which is located in the south of Turkey and is one of the important rivers of the region, has been selected as the study area. Göksu is a river flowing through the provinces of Antalya, Konya, Karaman and Mersin in Turkey with a length of 260 km and a basin area of approximately 10,000 km^2. Göksu originates from the Middle Taurus Mountains in two arms. The southern branch originates from the Geyik Mountains, and the northern branch originates from the Haydar Mountains and merges within the borders of the Mut District. From its confluence, the river takes the name Göksu, and then it empties into the Mediterranean Sea in the south of Silifke District. This study aims to investigate the temporal changes of Göksu River by using remote sensing methods. In the study, the Normalized Difference Water Index (NDWI) was used for the extraction of water bodies. In addition, the Normalized Difference Vegetation Index (NDVI) was used to study the temporal changes of forest and agricultural areas along the river line.

1. Introduction

Rivers provide water for irrigation, domestic supply, power generation and industry as well as a range of other ecosystem services and intrinsic and biodiversity values. Managing rivers to provide multiple benefits is therefore foundational to water security and other policy priorities. Rivers, which have become a religious symbol in some ancient societies, also play a big role in the vegetation changes around them. In this study, the temporal change of the Göksu River has been studied based on more than one year in recent seasons. In addition, the density of vegetation grown in the riparian region of the riversides and its change in time was studied.

1.1. Remote Sensing Data and Source

Remote sensing is the process of detecting and monitoring the physical characteristics of an area by measuring its reflected and emitted radiation at a distance (typically from satellite or aircraft). The Landsat series is a joint USGS and NASA-led enterprise for Earth Observation that represents the world's longest running system of satellites for moderate-resolution optical remote sensing for land, coastal areas, and shallow waters. Landsat satellite data has important advantages in monitoring and evaluating long-term land changes (Gülci et al. 2019). After the launch of the first Landsat satellite (Landsat 1) in 1972, the series from 1 to 9 has followed until today. The Landsat 6 satellite was

Cite this;

Satılmış, H., Çorumluoğlu, Ö. & Akyel, E. (2023). Temporal Change of Göksu River. Advanced Geomatics, 3(2), 72-81.

destroyed during launch. In this study, Landsat 4-5 TM C1 Level-1 data and Landsat 8 OLI/TIRS C1 Level-1 were downloaded freely from the USGS Earth Explorer site. Landsat satellite data can be downloaded from the EarthExplorer USGS site at no cost (Kayalık and Çorumluoğlu 2022). Land and scene cloud cover were chosen to be less than 3%. There are two types of image data available for the Landsat 4-5 satellite: MultiSpectral Scanner (MSS) and Thematic Mapper (TM). In addition to this, TM sensor with its seven spectral bands provides more radiometric information than the MSS sensor. TM, which has been used since 1984, has six bands with 30m resolution and Thermal Band with 120m resolution in the visible NIR and SWIR region. See Table 1.

Table 1. Landsat 4-5 TM band specifications.

TM Bands	Wavelength micrometers)	Resolution (meters)
B (Blue)	0.45 - 0.52	30
G (Green)	0.52 - 0.60	30
R (Red)	0.63 - 0.69	30
Near infrared	0.76 - 0.90	30
Mid-infrared	1.55 - 1.75	30
Thermal infrared	10.40 - 12.50	120
Mid-infrared	2.08 - 2.35	30

Landsat 8 OLI/TIRS carries two different devices: OLI (Operational Land Imager) and TIRS (Thermal Infrared Sensor). Besides the previous conventional bands, OLI (Operational Land Imager) includes a deep blue band for coastal/aerosol studies, a short-wave infrared band for the detection of sirrus clouds and a quality assessment band. The TIRS (Thermal Infrared Sensor) sensor has two thermal bands. These sensors provide a radiometric resolution of over 12bit of signal-to-noise radiometric performance. These 12 bits provides 4096 potential gray color levels compared to 256 gray level colors of 8 bit. The products are delivered in 16-bit. The Landsat 8 OLI/TIRS satellite, launched in 2013, has eight bands with a resolution of 30m, a PAN band with a resolution of 15m and 2 bands with a resolution of 100m. See Table 2.

Table 2. Landsat-8 OLI/TIRS band specifications

Bands	Wavelength (micrometers)	Resolution (meters)
Coastal aerosol	0.43 - 0.45	30
Blue	0.45 - 0.51	30
Green	0.53 - 0.59	30
Red	0.64 - 0.67	30
Near Infrared(NIR)	0.85 - 0.88	30
SWIR 1	1.57 - 1.65	120
SWIR 2	2.11 - 2.29	30
Panchromatic	0.50 - 0.68	15
Cirrus	1.36 - 1.38	30
Thermal Infrared(TIRS) 1	10.60 - 11.19	100
Thermal Infrared(TIRS) 2	11.50 - 12.51	100

In this study, multi-spectrum satellite images from Landsat-5 (TM) and Landsat-8 (OLI / TIRS) satellites were downloaded as time series data to detect water in riverbed and vegetation coverage in the riparian area of Göksu river in time. Therefore, starting from 2000, a total of 8 images were downloaded at intervals of two or three years until 2021. Eight images downloaded were selected from the season covering July, August, and September, but were downloaded from August in general. For the accuracy of the project, the cloudiness of the downloaded images was chosen to be less than 3%.

1.2. Study Area

The part where Göksu River flows into the Mediterranean Sea from within the borders of Mersin province was chosen as the study area. Due to many reasons, such as the amount of precipitation, underground resources, global warming, changes may occur in the river areas. In addition, it is considered that the Ermenek Dam, which is located close to the study area, may have an effect on the temporal change of the Göksu River. Ermenek Dam is located on the Göksu River and was opened in 2009. Geographical location of study area lies between 36° 12 to 36° 37 N and between 33° 12 to 34° 2 E. Location map was prepared for the determined are Fig. 1.

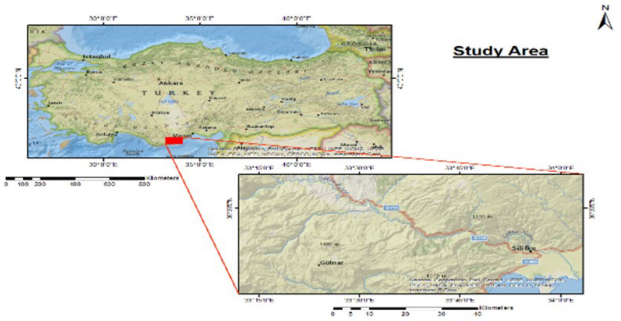

Figure 1. Location map of the study area

2. Material and Method

In the previous sections, the river area, the vegetation area and their indices were explained and some information about data acquisition is also given. In this section, information about the materials and methods used is explained. The temporal changes of the region (river for water area and river banks for vegatation cover), so riparian area of Göksu river selected as the study area is being studied. Images of the study area have been downloaded for free from the USGS Earth Explorer site, from the Landsat-5 and Landsat-8 satellites. Dark Object Subsraction (DOS) and Conversion of the Digital Number to Top of Atmosphere Reflectance (DN to ToA Reflectance) operations were applied to the downloaded data. NDWI-Normalized Difference Water Indexes were used for the river area extraction and NDVI-Normalized Difference Vegetation Indexes were used for the vegetation area extraction in yearly maner. Then, Unsupervised Classification was performed on the images with the indexes applied. After the classification, the temporal changes of the river and vegetation areas were examined, and then accuracy assessment was performed.

2.1. Image Processing

Landsat data has been used in change analysis studies for decades because of its relatively high spatial resolution covering long-term intervals. Change analysis with remote sensing techniques is the process of determining temporal differences between images. In this process, while electromagnetic radiation detected by various sensors travels from the earth's surface to the sensing sensor, gases, aerosols and other atmospheric components are exposed to atmospheric effects (such as scattering and absorption) by atmospheric components. Radiometric distortions occur due to the changes in the light falling on the images, the geometry of the view, atmospheric conditions and the response time of the sensor. Some atmospheric and radiometric corrections need to be applied to satellite images in order to minimize the resulting system errors and to eliminate the distortions caused by atmospheric particles.

2.1.1. Data Calibration

Thanks to data calibration, the differences in the data obtained in different systematic scenario situations at different times are eliminated in the form of digital records of a physical phenomenon, and comparable meaningful reflectance values are obtained. The formulas used in the calibration of the data are given below as indicated by Equation 1.a, 1.b, 2 and 3.

$$L_\lambda = ((L_{MAX\lambda}-L_{MIN\lambda})/(Q_{CALMAX}-Q_{CALMIN}))*(Q_{CAL}-Q_{CALMIN})+L_{MIN\lambda} \quad (1.a)$$

$$\rho_\lambda = (\pi * L_\lambda * d^2) / (ESUN_\lambda * \cos\theta_S) \quad (1.b)$$

$$\rho_\lambda' = M_\rho * Q_{cal} + A_\rho \quad (2)$$

$$\rho_\lambda = \rho_\lambda'/\cos(\theta_{SZ}) = \rho_\lambda' / \sin(\theta_{SE}) \quad (3)$$

Here, Lλ = ToA spectral radiation-radiance (Watts / (m^2 x srad x μm)), Qcal = Pixel values (DN), Mρ = Image channel specific multiplicative rescaling factor, Aρ = Image channel specific additive rescaling factor, ρλ = ToA reflectance value, θSE = Sun elevation angle, θSZ = Sun zenith angle ; θSZ = 90° - θSE.

2.1.2. Atmospheric Correction

Atmospheric correction is simply defined as the process of removing atmospheric effects from satellite images. Some atmospheric and radiometric corrections should be applied to satellite images in order to minimize the resulting system errors and to eliminate the distortions caused by atmospheric particles (Bektaş Balçık and Gölsel 2010; Liang 2004).

2.2. Normalized Difference Water Index (NDWI)

The normalized difference water index (NDWI) is a method developed to describe open water features and improve their presence in remotely sensed digital images. NDWI utilizes reflected near-infrared radiation and visible green light to highlight the spectral characteristics of water while removing soil and terrestrial vegetation features. This band ratio approach is calculated by Equation (5) given below (Xu 2022).

$$NDWI=Green-NIR/Green+NIR \quad (5)$$

Here, Green Band: 0.519 μ - 0.601 μ wavelength range for Landsat 5 sensor, 2nd band; For the Landsat 8 sensor, it has a wavelength range of 0.533μ - 0.590μ and corresponds to the 3rd band. NIR (Near Infrared): For Landsat 5 sensor, it is in the wavelength range of 0.772 μ - 0.898 μ, in Band 4; For Landsat 8 sensor, it is 0.851 μ-0.879 μ, corresponding to the 5th band.

2.3. Normalized Difference Vegetation Index (NDVI)

Normalized Difference Vegetation Index (NDVI) is a band ratio technique developed to estimate the size of vegetation biomass. NDVI is calculated using the formula given in Equation (6).

$$NDVI=NIR-Red/NIR+Red \quad (6)$$

Here, NIR (Near Infrared): For Landsat 5 sensor, it is in the wavelength range of 0.772 μ - 0.898 μ, in Band 4; For Landsat 8 sensor, it is 0.851 μ-0.879 μ to the 5th band; Red Band: For Landsat 5 sensor it has a wavelength range of 0.631 μ - 0.692 μ and corresponds to the 3rd band, for Landsat 8 sensor it is in the range of 0.636 μ-0.673 μ and corresponds to the 4th band.

2.4. Image Classification

Digital image classification is the process of clustering all the pixels belonging to the relevant image into classes in an assigned number. In a multiband optical image composed of pixels, each pixel defines the reflectance values of the part of the object associated with the pixel, obtained along the bands. Classifications made by determining only the number of classes are called unsupervised classification, while classifications made by determining the classes with the help of a training set are called supervised classification. As the classes assigned on the image can be determined by the user, it can also be done randomly by specifying only the number of classes (Lillesand et al. 2007). Unsupervised classification method was used in this study.

2.5. Accuracy Analysis

For the reliability of the images produced as a result of the classification, which performs the algorithms cyclically, the accuracy of the operations performed must be tested.

2.6. Change Determination

It is the process of comparing and interpreting the values obtained as a result of the analyzes performed on the satellite images.

3. Results and Discussion

In this part of the study, the results obtained as a result of the application of the techniques given in the previous section will be shared. First of all, necessary preprocessing steps were applied on the satellite images of the Göksu River area. The results obtained as a result of NDWI, NDVI and classification, which are evaluated within the scope of the study, will be shared on the satellite images prepared for analysis by applying preprocessing steps.

3.1. Image Preprocessing

Image preprocessing is a step that involves performing the necessary calibration processes for the data remotely sensed by a sensor and thus eliminating the systematic errors that occur. Many techniques have been developed to remove atmospheric distortions, including image-based dark object extraction (Chavez 1988) techniques. In this study, radiometric calibration and atmospheric correction processes were performed. From the images obtained within the scope of this process, first the brightness value and then the reflection value were obtained by using the data in the metadata file (data collection date, sun height, azimuth angle, etc.) in the satellite images. At the end of the processing steps, new images were produced covering the entire workspace, minimizing possible errors. The raw satellite image shown in Fig. 2, arranged in Fig. 3 is shown.

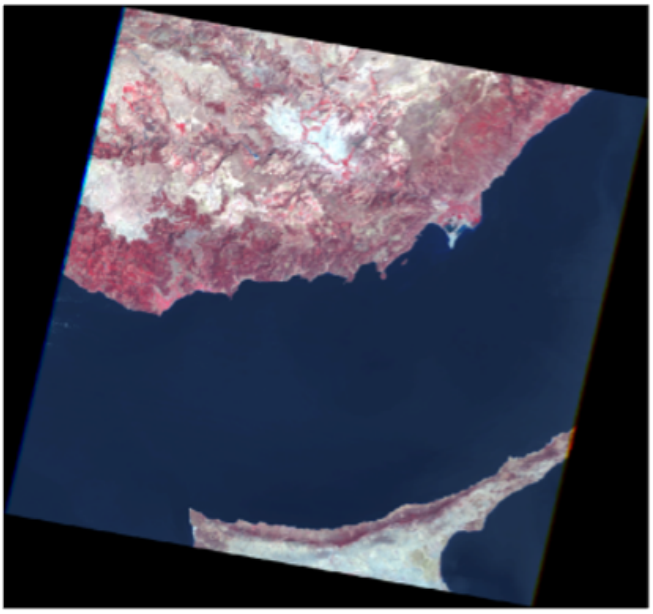

Figure 2. Raw Satellite Image

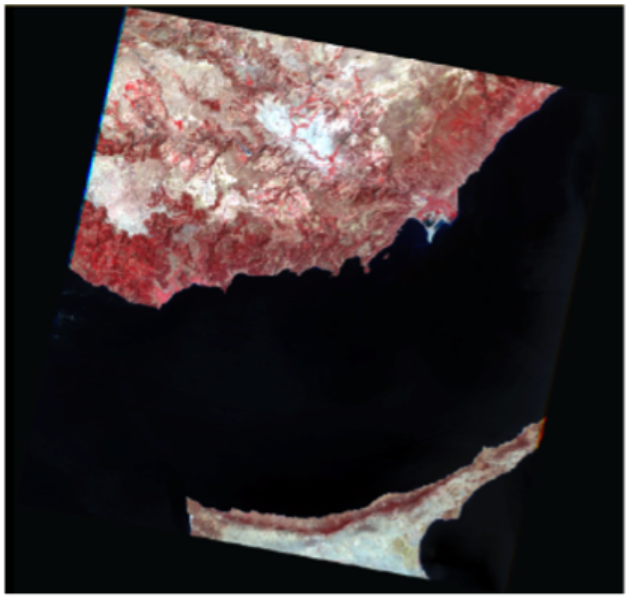

Figure 3. Processed Satellite Image

3.2. Normalized Difference Water Index (NDWI)

NDWI, which is calculated by incorporating satellite images into the analysis, is widely used in the detection and mapping of surface water bodies. The findings obtained as a result of the NDWI procedure are given in Fig. 4.

Figure 4. NDWI image of 26th July 2016

3.3. Normalized Difference Vegetation Index (NDVI)

Normalized Difference Vegetation Index (NDVI) was used to describe the surface vegetation of the regions. The NDVI is among the prosperous methods used for the extraction vegetation from satellite images. The findings obtained as a result of the NDVI procedure are given in Fig. 5.

Figure 5. NDVI image of 26th July 2016

3.4. Unsupervised Classification

It is the process of producing thematic maps with the help of images by gathering objects with the same spectral reflectance properties in the spectral reflectance feature space defined by bands under the same class (Doğan 2008). In the continuation of the processes, unsupervised classification was performed on the satellite images of the Göksu River. The maps of Göksu River Water class and vegetation class obtained as a result of classification are given in Fig. 6 and Fig. 7, respectively.

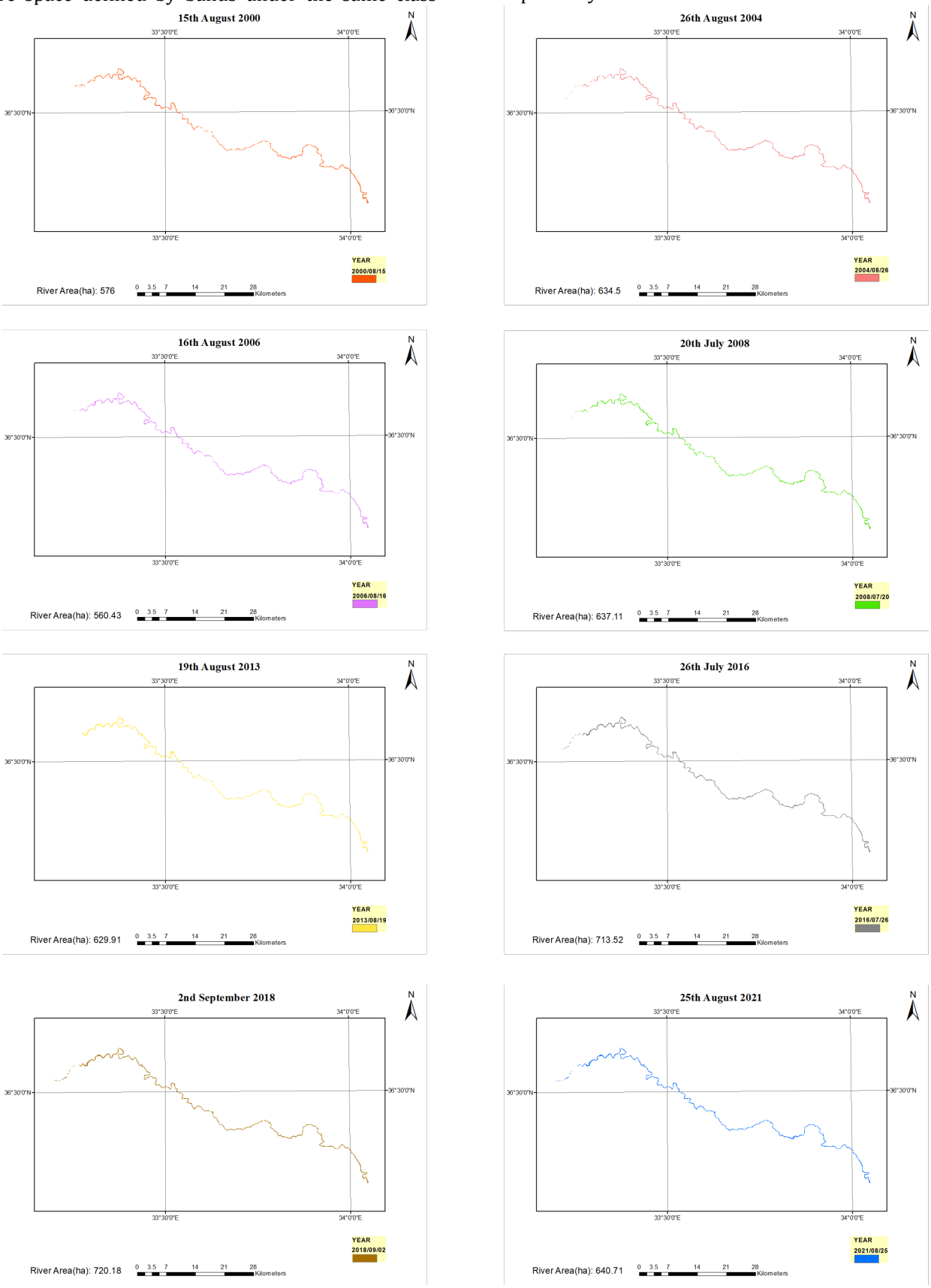

Figure 6. Classified Map of River Area

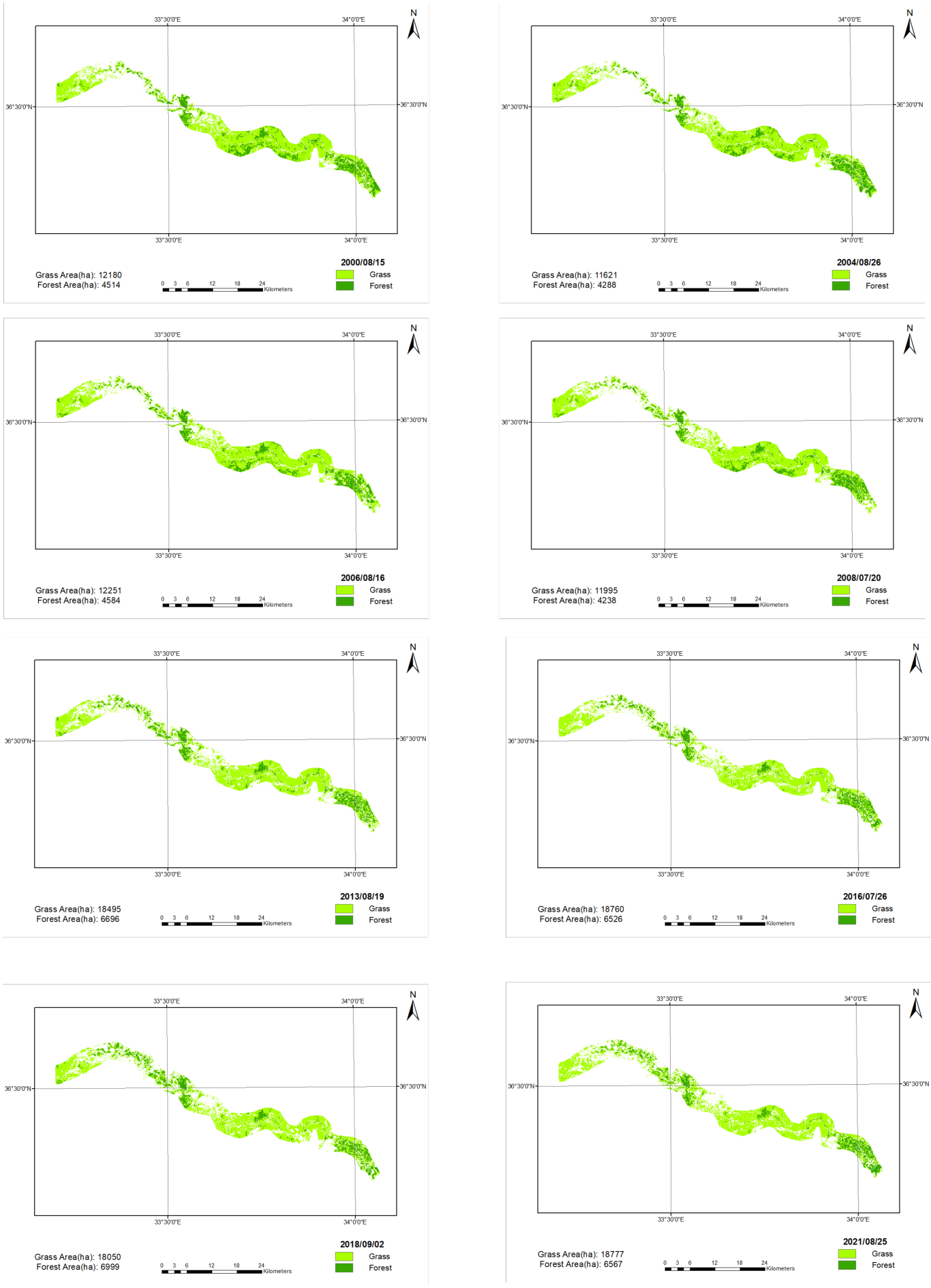

Figure 7. Classified Map of Vegetation Area

3.5. Accuracy Assessment

Determining the wavelength to be used in the unsupervised and supervised classification process, the sufficient accuracy and number of control areas, the classification algorithm and testing its accuracy are extremely important for the reliability of the actual study (Örmeci and Ekercin 2005). Testing the accuracy of the classification, the data produced It is based on the principle of statistically checking its accuracy. Accuracy analysis of the classification process applied to the Göksu River was carried out. Accuracy analysis was performed using the error matrix method. The findings obtained as a result of the analysis are as given in Table 3.

3.6. Change Determination

Within the scope of the study, satellite images of Göksu River were made comparable after all processing steps that would allow interpretation. Then, the changes of vegetation and river areas were determined. River Area changes are given in Fig. 8, Vegetation Area changes are given in Fig. 9.

Table 3. Accuracy Rate of River and Vegetation Region

Dates	Accuracy Rate of	
	River Region	Vegetation Region
15th August 2000	80.00%	87.00%
26th August 2004	84.00%	83.00%
16th August 2006	83.00%	87.00%
20th July 2008	85.00%	93.00%
19th August 2013	92.50%	88.00%
26th July 2016	93.75%	89.00%
2nd September 2018	97.50%	84.00%
25th August 2021	90.00%	82.00%

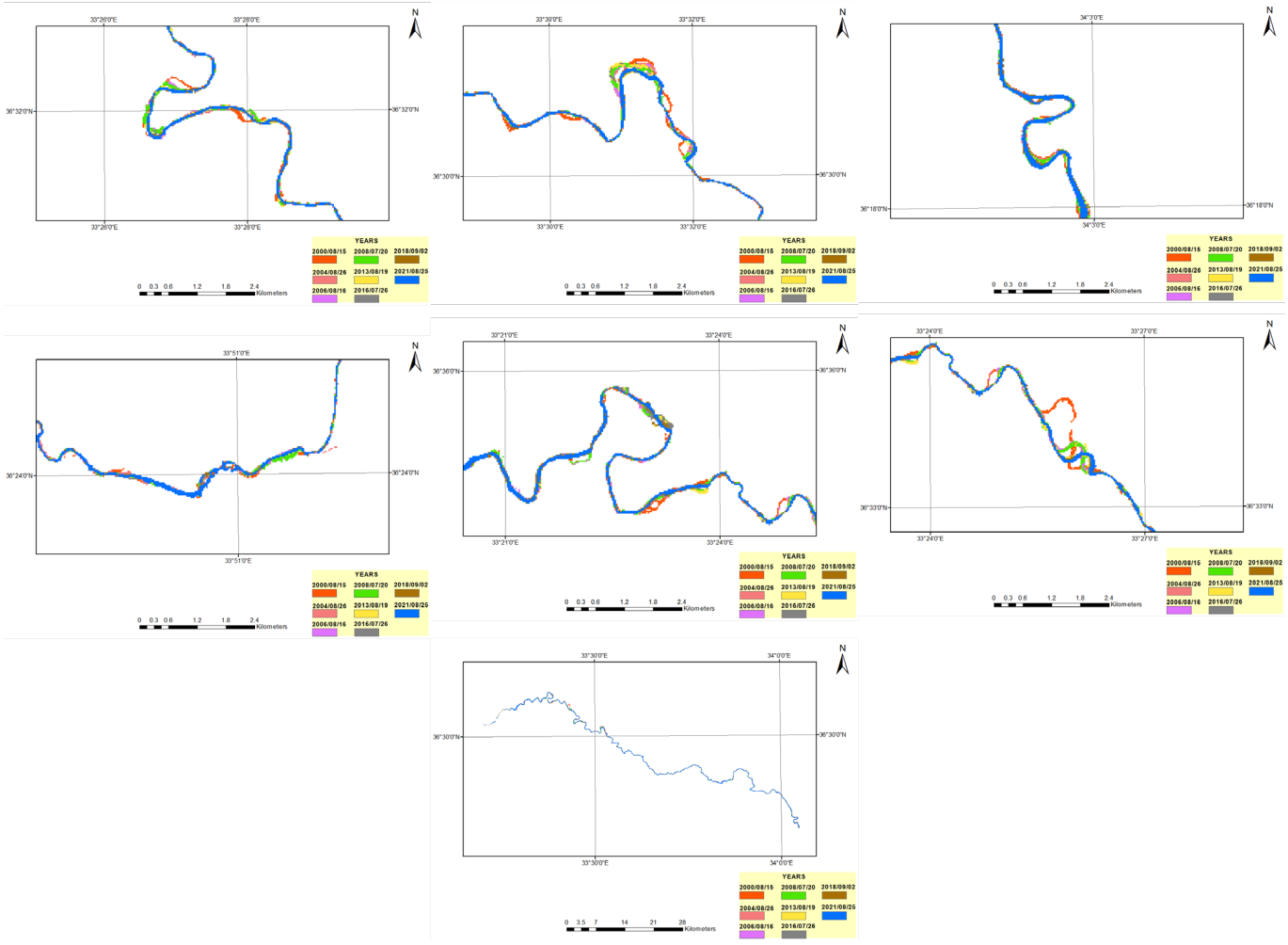

Figure 8. River Area Change Detection

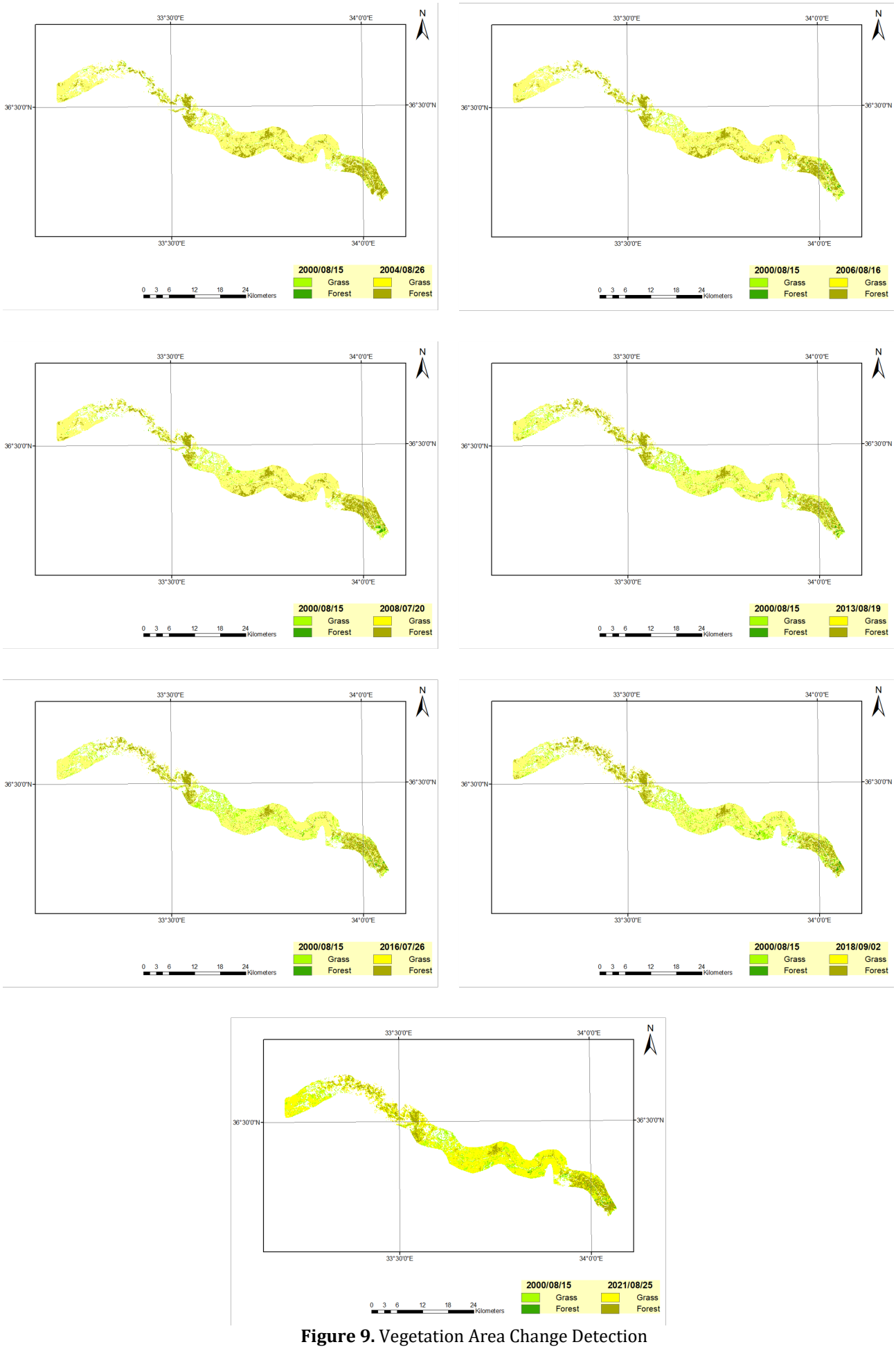

Figure 9. Vegetation Area Change Detection

As a result of the change analyzes applied, the change of the area of the river according to the years is given in Table 4 and Fig. 10.

Table 4. River Areas by years

Date	River Area(ha)
2000/08/15	576.00
2004/08/26	634.50
2006/08/16	560.43
2008/07/20	637.11
2013/08/19	629.91
2016/07/26	713.52
2018/09/02	720.18
2021/08/25	640.71

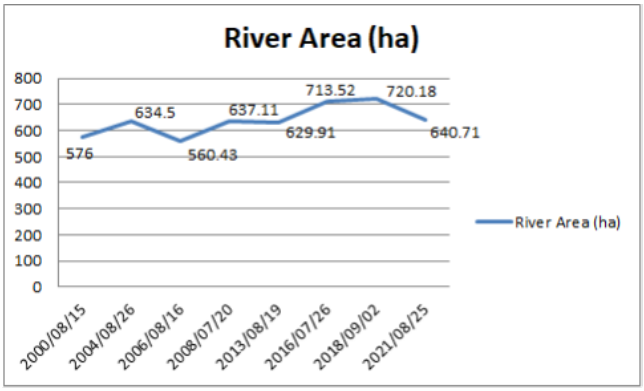

Figure 10. Graph of River Area by years

As a result of the change analyzes applied, the change of the area of the vegetation according to the years is given in Table 5 and Fig. 11.

Table 5. Grass and Forest Areas by years

	Grass Area(ha)	Forest Area(ha)
2000/08/15	12180	4514
2004/08/26	11621	4288
2006/08/16	12251	4584
2008/07/20	11995	4238
2013/08/19	18495	6696
2016/07/26	18760	6526
2018/09/02	18050	6999
2021/08/25	18777	6567

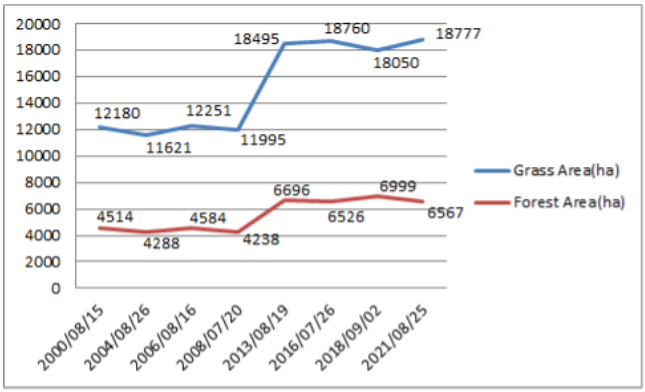

Figure 11. Graph of Grass and Forest Areas by years

4. Conclusion

In our country, remote sensing technology is widely used in monitoring wetlands and detecting changes over time (Özçalık et al. 2020). Monitoring lake areas is a relatively new science. Climate change, excessive water use, etc. For these reasons, the lakes are under the threat of drought (Kaplan et al. 2016). In this study, the 260 km long Göksu River, which is a river flowing through the provinces of Antalya, Konya, Karaman and Mersin and pouring into the Mediterranean in the south of Silifke district of Mersin province, was chosen as the analysis area. Analyzes were carried out using Landsat satellite images and multi-band satellite images recorded by satellite sensors were evaluated for the purpose of examining lake surface water. Satellite technologies, which provide spatial information about certain characteristics of lakes, offer services that can complement ground-based monitoring programs at lower cost (Cüce and Bakan 2009). Firstly, the satellite images, which were subjected to image preprocessing steps, were made ready for analysis after necessary corrections were made. The change of the Göksu River surface water over the years was examined through the satellite images that were prepared for analysis.

Data for the years 2000, 2004, 2006, 2008, 2013, 2016, 2018 and 2021 have been downloaded. The downloaded data are for the months of July, August and September. While downloading the data, it was preferred that the dates be close to each other in terms of day and month. NDWI, NDVI and unsupervised classification images were obtained with images cut from this data. The threshold value applied during the processing of the indices was chosen according to the pixel values of the water and vegetation in the image. Images with applied NDWI and NDVI indices were used for unsupervised classification. During unsupervised classification, images were divided into 2 classes to separate the river area and 5 classes to separate the vegetation area. Of these 2 classes, 1 was chosen as a river and 2 out of 5 classes was chosen as a vegetation area. Accuracy assessments and area calculations were made on the classified data. The accuracy rate for the river area has ranged from 80% to 97.50% over the years. For vegetation, it was between 82% and 93%. And these results are quite satisfactory for this project. It was determined that the reason for the low level of riverbed change in the southeast part of the study area was urbanization. Likewise, it was determined that the forest area in the same region was mostly the parcels where fruit and vegetable trees were grown. Apart from these, it is thought that one of the reasons for the change in the riverbed is the Ermenek Dam, which was opened in 2009.

Funding

This research received no external funding.

Author Contributions

Hakan Satılmış: Conceptualization, Methodology, Visualization, Investigation, Writing
Özşen Çorumluoğlu: Reviewing and Editing, Investigation
Elif Akyel: Writing-Original draft preparation, Data curation, Visualization, Writing-Reviewing and Editing.

Conflicts of Interest

The authors declare no conflicts of interest.

References

Balçık, F. B., & Göksel, Ç. (2009). SPOT 5 ve Farklı Görüntü Birleştirme Algoritmaları, 12. Türkiye Harita Bilimsel ve Teknik Kurultayı, 11, 15.

Chavez Jr, P. S. (1988). An improved dark-object subtraction technique for atmospheric scattering correction of multispectral data. Remote sensing of environment, 24(3), 459-479.

Cüce, H., & Bakan, G. (2009). Sürdürülebilir Su Kaynakları Yönetimi Açısından Uzaktan Algılama ve Coğrafi Bilgi Sistemlerinin Önemi. TMMOB Coğrafi Bilgi Sistemleri Kongresi, 2(06).

Doğan, İ. (2008). Uzaktan algılama verileri ile kıyı çizgisi değişiminin zamansal olarak belirlenmesi: Alaçatı örneği. Master Thesis, Yıldız Technical University, Graduate School of Science and Engineering, İstanbul, Türkiye.

Gülci, S., Gülci, N., & Yüksel, K. (2019). Monitoring water surface area and land cover change by using Landsat imagery for Aslantaş Dam Lake and its vicinity. Journal of the Institute of Science and Technology, 9(1), 100-110.

Kaplan, G., Avdan, U., Avdan, Z. Y., & D Yildiz, N. (2016). Landsat uydu görüntüleri kullanılarak kuraklık izlenmesi (Akşehir gölü örneği). 6. Uzaktan Algilama-CBS Sempozyumu. Adana, Türkiye.

Kayalik, M., & Çorumluoğlu, Ö. (2022). SST Correlation Between Chlorophyll and Turbidity by Landsat MS Image Analysis for the Coast of Izmir Province. International Journal of Environment and Geoinformatics, 9(4), 35-45.

Liang, S. (2005). Quantitative remote sensing of land surfaces. John Wiley & Sons.

Lillesand, T., Kiefer, R. W., & Chipman, J. (2015). Remote sensing and image interpretation. John Wiley & Sons.

Örmeci, C., & Ekercin, S. (2005). Uzaktan Algilama Tekniği ile Tuz Gölünde Su Kalitesi Değişim Analizi, 10. Türkiye Harita Bilimsel ve Teknik Kurultayı, Ankara, Türkiye.

Özçalık, H., Torun, A. T., & Bilgilioğlu, S. S. (2020). Landsat uydu görüntüleri kullanılarak Mogan Gölü'nün su yüzeyi ve arazi örtü değişiminin belirlenmesi. Türkiye Uzaktan Algılama Dergisi, 2(2), 77-84.

Xu, H. (2006). Modification of normalised difference water index (NDWI) to enhance open water features in remotely sensed imagery. International journal of remote sensing, 27(14), 3025-3033.